Phosphorylation Based Insulation Devices Design and Implementation

by

Phillip M. Rivera Ortiz

Submitted to the Department of Mechanical Engineering
in partial fulfillment of the requirements for the degree of

Master of Science in Mechanical Engineering

at the

MASSACHUSETTS INSTITUTE OF TECHNOLOGY

June 2013

Author .....
Department of Mechanical Engineering
May 10, 2013

Certified by .....
Domitilla Del Vecchio
Associate Professor
Thesis Supervisor

Accepted by .....
David E. Hardt
Chairman, Department Committee on Graduate Theses

Phosphorylation Based Insulation Devices Design and Implementation

by

Phillip M. Rivera Ortiz

Submitted to the Department of Mechanical Engineering
on May 10, 2013, in partial fulfillment of the
requirements for the degree of
Master of Science in Mechanical Engineering

Abstract

This thesis presents the analysis of a phosphorylation based insulation device implemented in *Saccharomyces cerevisae* and the minimization of the retroactivity to the input and retroactivity to the output of a single cycle phosphorylation device by means of optimal substrate and phosphatase concentration selection. Characterizing and improving the performance of insulation devices brings us a step closer to their successful implementation in biological circuits, and thus to modularity. To this end, an insulation device was designed and implemented in *Saccharomyces cerevisae* employing the principle of timescale separation. It was shown experimentally (data pending publication), that the dynamics of the insulation device output remained unchanged in the presence of promoter sites (load) providing retroactivity.

In this thesis, the underlying mechanism by which the insulation device retains its dynamic performance in the presence of load is explained through singular perturbation and parameter sensitivity analysis. It was determined that the fast phosphotransfer reactions of the insulation device indeed allowed for retroactivity attenuation provided the substrate and phosphatase concentration are in sufficient amounts. Furthermore, the retroactivity to the input and retroactivity to the output of phosphorylation based insulation devices were parameterized with the substrate and phosphatase concentrations using a single cycle model. While previous works have focused on showing output retroactivity attenuation through high substrate and phosphatase concentration, it is shown that this has detrimental effects on the insulation device performance even in isolation. Employing singular perturbation and contraction theory tools, this work provides a framework to determine an optimal substrate and phosphatase concentration to reach a tradeoff between the retroactivity to the input and the retroactivity to the output.

Thesis Supervisor: Domitilla Del Vecchio
Title: Associate Professor

Acknowledgments

I would not have been able to have this great chance to work in such an interdisciplinary effort without my collaborators. I want to take this opportunity to acknowledge them as well as the people who have guided and helped me throughout this process.

First I would like to thank my advisor Domitilla Del Vecchio for her guidance and giving me the opportunity to work on an applied project stemming from our theoretical efforts. Also I would like to thank Ron Weiss and Deepak Mishra for their wonderful work on designing and building the insulation device in yeast. Specifically I would like to thank Deepak for his sleepless nights in the lab doing all the experiments needed for the validation of the insulation device design and providing all the data needed for the presented analysis. I would also like to thank all my colleagues in the Del Vecchio group for all the interesting discussions and help throughout these two years.

Ahora me gustarìa agradecer a toda mi familia "Bostoniana" incluyendo a: Baldin, Juan, Edward, Melyorise, Francine, Carlos, Diamilet, Yamil, Enrique y C.J.. Ustedes hacen que la experiencia valga la pena, no podrìa pedir un mejor/"funcional" grupo de amigos. Ademàs a Bàrbara por su entendimiento y apoyo durante este tiempo. Finalmente le quiero agradecer a mi madre por darme la habilidad de soñar. Two down, one to go!

Contents

List of Figures

List of Tables

Chapter 1

Introduction

Understanding modularity is one of the most pressing matters in systems biology. Modularity is the property according to which the input/output behavior of a system does not change upon interconnection and has been proposed as one of the possible levels of biological organization [1]. It was suggested, however, that biomolecular systems are not always modular because impedance-like effects at the interconnections, called retroactivity, alter the system's behavior [2] [3] [4]. Figure 1-1 shows the system model introduced in [2] to explicitly account for retroactivity. System Π, with input u and output y, is subject to retroactivity to the output s, due to interconnection to a downstream system, and applies retroactivity to the input r to its upstream system. In a biological circuit, this occurs, for example, when a protein is used as a transcription factor. The downstream process uses the protein in its reactions, directly affecting its dynamics. Retroactivity has also been related to fan-out [5], which is defined as the maximum regulation capacity of a transcription factor.

Figure 1-1: System model with retroactivity signals. System Π with input u, output y, retroactivity to the input r and retroactivity to the output s.

1.1 What is an insulation device?

From an engineering point of view, an insulation device can be used to decouple the dynamics of interconnected components. This device is analogous to an insulating amplifier in electrical circuits, where a signal is transmitted to a downstream system while minimizing the impedance effects. Similarly, an ideal insulation device has the retroactivity to the input r in Figure 1-1 close to zero and the effect of the retroactivity to the output s on y is completely attenuated. The realization of devices with these characteristics have been proposed and implemented in ad-hoc ways in the synthetic biology context. For example, it has been suggested that signaling pathways, such as the mitogen-activated protein kinase (MAPK) cascade, can be used as amplifiers and placed in negative feedback loops to obtain insulation from downstream loading [6]. And, implementations of insulation devices have been realized *in vitro*, where the dynamics of a biological oscillator were successfully decoupled from the dynamics of "DNA tweezers" using a "genelet" amplifier circuit [7].

1.2 Insulation device design principles

There exists a mathematical treatment of systems with the retroactivity attenuation property, as it was shown in [8] that an insulation device can be constructed employing the principle of separation of timescale. Conceptually, the principle is implemented by placing a fast process between a slow input and the downstream clients. This decouples the dynamics of the input module from the dynamics of the downstream clients (load) independent of their demand. The approached used in [9] is based on Tikhonov's theorem of singular perturbation and the main result suggests that if the internal dynamics of the insulated system are fast enough, their quasi steady state dynamics can be isolated from the effects downstream clients and depend only on the slow input to the system, thus attenuating retroactivity effects to the output. A device exploiting this principle was successfully constructed and implemented in *Saccharomyces cerevisae*, making it the first systematic design of such a device realized

in vivo. The system was constructed using a transcriptional activation stage as the slow input, whose timescale in the order of minutes [10], and a phosphorylation cycle cascade as the fast internal process, whose protein-protein phosphotransfer reactions have a timescale in the order of seconds [11].

Furthermore, it was shown [3] that phosphorylation cycles can attenuate retroactivity to the output through a mechanism similar to high gain feedback even without an explicit negative feedback. And indeed, in vitro implementations have confirmed this theoretical prediction [12]. As described in [3] the key tunable parameters of a phosphorylation based insulation device are the substrate and phosphatase concentration, and as they are increased, the effect of the retroactivity to the output on the cycle output protein could be attenuated. However, increased amounts of cycle substrate result in an increased retroactivity to the input, placing a fundamental tradeoff between the minimization of the input retroactivity and the output retroactivity. Thus, the optimal design of a phosphorylation based insulation device requires the substrate and phosphatase concentrations to be implemented in a specific range to mitigate both retroactivity effects.

1.3 Thesis content

Two main topics are addressed in this thesis. First, a mathematical description of how the principle of separation of timescale is successfully implemented to design an insulation device based on transcriptional activation and a phosphotransfer cascade is provided. Second, an expression for the optimal substrate and phosphatase concentration in a phosphorylation based insulation device that minimizes the retroactivity to the input and retroactivity to the output of an insulated system is derived using tools from nonlinear systems theory.

The thesis main narrative is divided into two chapters, one addressing each of the previously described topics. The first chapter titled "Implementation of an insulation device based on time scale separation" presents the analysis of a system with an insulation device that was designed based on the separation of timescale princi-

ple and implemented in *Saccharomyces cerevisae.* The presented analysis proves this insulation device fits the class of systems presented in [8] and thus has the retroactivity attenuation property. Its dynamic performance is assessed by comparing the biological circuits performance to a circuit with the same transcriptional activation input and load, but lacking the insulation device (called uninsulated system). Using a green fluorescent protein (GFP) in both systems as a reporter, flow-cytometry data was collected to measure the response of the system to step up, step down and time varying inputs. Using the experimental data (not shown-pending publication) the model parameters were fitted and the characterization of the insulation device was done through: the application of singular perturbation; calculating the trajectory error for simulated changes in substrate and phosphatase concentrations, and changes in the time scale of the insulated system phosphotransfer dynamics; and a dynamic and steady state sensitivity analysis. The chapter is organized as follows. In Section 2.1 the insulated and uninsulated system constructions and models are presented, including the chemical reactions considered and their underlying assumptions. The parameter fit results and input signal design for the dynamic experiments is also included. In Section 2.2 the mathematical explanation of the retroactivity attenuation mechanism is described in terms of singular perturbation, including an assessment of the stability of the slow manifold. Section 2.3 includes a qualitative explanation of the retroactivity attenuation property based on a flux analysis of the quasi steady state approximation. The results of a steady state and dynamic sensitivity analysis are included in Section 2.4. Also, the load drivers performance is studied under various phosphorylation time scales for a range of loads, as well as its performance for different substrate and phosphatase concentrations subjected to the same range of loads. Section 2.5 contains a discussion of this analysis.

The second chapter titled "Tradeoffs in the design of insulation devices" presents a parameterization of the error of an insulation device based on a single phosphorylation cycle with the cycles substrate and phosphatase concentrations. Their optimal concentrations that minimize the retroactivity to the input and retroactivity to the output are determined. The analysis is performed using tools from contraction the-

ory to provide a mathematical expression for an upper bound in the error between the insulated loaded and unloaded system under varying substrate and phosphatase concentrations. This chapter is organized as follows. In Section 3.1, the mathematical tools needed for the problem solution are provided. In Section 3.2, the system model and problem are presented in terms of the chemical reactions and differential equations describing the phosphorylation cycle. Also, the definition of the input error and output error of the insulation device are given. In Section 3.3, a general solution approach using model reduction techniques is presented. Sections 3.4 and 3.5 provide the input and output error in terms of the cycle substrate and phosphatase concentrations. In Section 3.6, the total error of the insulation device is provided. Section 3.7 provides a discussion of the presented analysis. Finally, Chapter 4 contains the conclusions including the required temporal features and parametric constrains for the successful design and implementation of insulation devices.

Chapter 2

Implementation of an insulation device based on time scale separation

The timescale separation principle described in [8] was used to design and build an insulated system in *Saccharomyces cerevisae.* This principle was applied by coupling a slow transcriptional stage, termed input device, to a phosphorylation cycle serving as the fast internal dynamics, called the insulation device. The output protein of the insulation acts as a transcription factor of a promoter expressing a fluorescent protein, thus the activation of this promoter is termed the system output. In order to measure the insulation device retroactivity attenuation property, a second system was built without the insulation device, but preserving the same input device and system output as the insulated system, termed the uninsulated system. More specifically, looking at Figure 2-1 and Figure 2-2, the input device of both systems consists of the induced expression of the P_{TET} promoter by the constitutively expressed reverse tetracycline transactivator protein (rtTA) in the presence of the small molecule doxycycline (DOX). The output stage consists of a chromosomally integrated $P_{TR-SSRE}$ promoter with 4 binding sites expressing the green fluorescent protein GFP. The idea of the experiment was to compare the system GFP output in isolation and in the presence of load (downstream binding sites) for both uninsulated and insulated

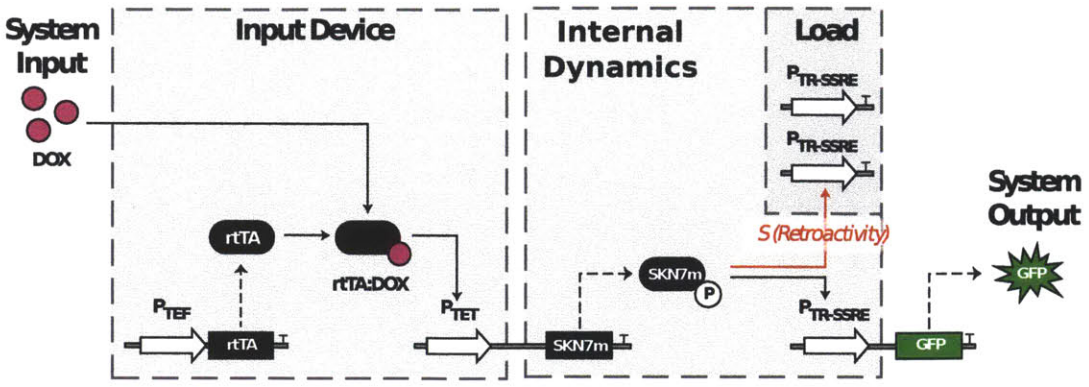

Figure 2-1: Uninsulated system circuit design. The system consists of the input device where the P_{TET} promoter is expressed by reverse tetracycline transactivator protein (rtTA) in the presence of doxycycline (DOX). The internal dynamics of the system include the expression and degradation/dilution of SKN7m, which is also the unbuffered system output protein. The load are the yeast high copy number plasmids with 800 binding sites of the $P_{TR-SSRE}$ promoter, while a chromosomally integrated $P_{TR-SSRE}$ promoter expresses the reporter protein GFP.

systems. Since both systems have the same input device and GFP output stage, the presence of the insulation device reactions in the insulated system is the only topological difference between the two. Thus if the dynamics of the insulated system remain unchanged in the presence of load, the insulation device design based on timescale separation indeed possessed the retroactivity attenuation property. The uninsulated system in Figure 2-1 has the P_{TET} promoter regulating the expression of SKN7m, an active mutant version of the endogenous SKN7 protein. SKN7m in turn activates the production of GFP through the $P_{TR-SSRE}$ promoter. To asses the dynamics of the uninsulated system due to binding to downstream clients, high-copy number 2μ yeast plasmids containing zero (unloaded) or two (loaded) additional copies of $P_{TR-SSRE}$ where included in the system. Thus, the dynamic performance of the uninsulated system was measured comparing the GFP dynamics for the unloaded case, where no additional $P_{TR-SSRE}$ binding sites are present, and for the loaded case containing 800 additional $P_{TR-SSRE}$ binding sites per cell. The dynamics of the SKN7m concentration, the internal dynamics of the system, are subjected only to protein production and decay which are inherently slow processes [REFERENCE], thus not possessing the retroactivity attenuation property through timescale separation as described in [8].

The insulated system in Figure 2-2 has the input device expressing the fusion protein STAT5-HKRR in the presence of DOX. The STAT5 domain of the fusion protein is phosphorylated by the JH1 domain of the constitutively expressed Janus kinase 2 (JAK2). This phosphorylated and unphosphorylated versions of STAT5-HKRR go through phosphotransfer interactions with the tyrosine phosphate dependent protein (YPD1). The phosphorylated form of YPD1 activates the endogenous SKN7 protein through double phosphorylation, and this double phosphorylated-SKN7 is able to activate the chromosomally integrated $P_{TR-SSRE}$ promoters leading to the expression of GFP. The phosphotransfer reactions in the insulated system comprise the insulation device and they provide the fast internal dynamics required for a system to achieve retroactivity attenuation property through timescale separation. The dynamics of the insulated system were also examined in the presence of the load through the addition

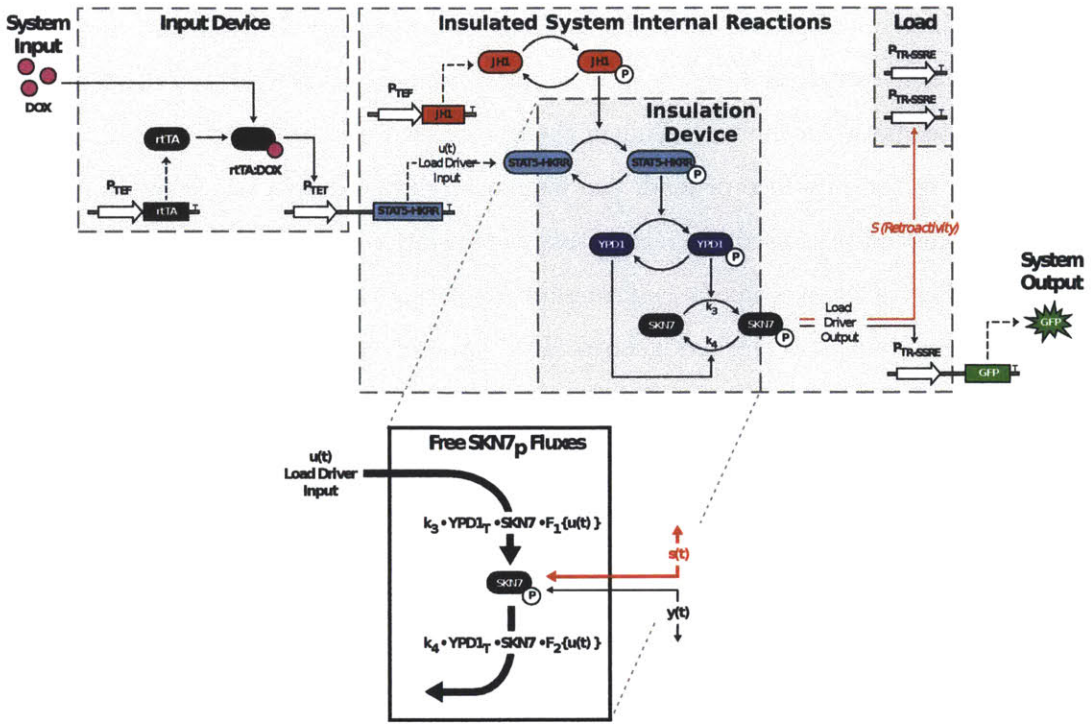

Figure 2-2: Insulated system circuit design. The system consists of the input device where the P_{TET} promoter is expressed by reverse tetracycline transactivator protein (rtTA) in the presence of doxycycline (DOX). The internal dynamics of the system include the expression of STAT5 and the constitutively expressed JH1, while the insulation device dynamics include all phosphotransfer reactions. The insulated system output is the double phosphorylated SKN7. The load are the yeast high copy number plasmids with 800 binding sites of the $P_{TR-SSRE}$ promoter, while a chromosomally integrated $P_{TR-SSRE}$ promoter expresses the reporter protein GFP.

of $P_{TR-SSRE}$ binding sites in yeast high copy number plasmids.

2.1 Mechanistic Model and Parameter Fit

2.1.1 Insulated and uninsulated system models

Mathematical models for the uninsulated and insulated circuits were developed to assess the dynamic and steady state effect of retroactivity on the concentration of transcription factors SKN7m (uninsulated circuit) and double phosphorylated SKN7 (insulated circuit) in the presence of load plasmids with $P_{TR-SSRE}$ promoters. Each system was written as a set of reactions governing protein species and then using mass action kinetics, formed into a set of Ordinary Differential Equations (ODEs). These ODEs were then used to construct a grey-box model using the MATLAB System ID Toolbox (The Mathworks, Natick, MA). Experimental datasets were used to fit parameters of the grey-box model using the Trust-Region-Reflective Least Squares algorithm. Final simulations were performed using a stiff differential equation solver (MATLAB `ode23s`) and final parameter values (Table B-1 & Table B-2).

2.1.2 Mathematical model formulation

Uninsulated system

The reactions considered in the uninsulated system are the DOX activated production of SKN7m from P_{TET}, the binding and unbinding of SKN7m to $P_{TR-SSRE}$ binding sites (load), the SKN7m activated production of GFP (reporter), and degradation/dilution of both SKN7m and GFP. Defining C_m as the complex formed between SKN7m and $P_{TR-SSRE}$ and $f_H(\cdot)$ denotes a production function, the reactions can be described by:

$$\phi \xrightarrow{f_H(DOX)} \text{SKN7m} \tag{2.1}$$

$$\text{SKN7m} + \text{p} \underset{k_{off}}{\overset{k_{on}}{\rightleftharpoons}} C_m \tag{2.2}$$

$$\text{SKN7m} \xrightarrow{\delta_X} \phi \tag{2.3}$$

$$\phi \xrightarrow{f_H(X_m)} \text{GFP}. \tag{2.4}$$

$$\text{GFP} \xrightarrow{\delta_G} \phi \tag{2.5}$$

To generate these reactions and the formation of subsequent ODEs, we make the following assumptions:

1. Reactions occur in single well-mixed compartment.

2. Extracellular DOX is in saturating conditions and there is rapid equilibrium between cytoplasm and extracellular media (DOX import and degradation can be neglected).

3. SKN7m does not dimerize or participate in other phosphorylation reactions due to mutation[13, 14].

4. The functions governing production of SKN7m and GFP (denoted $f_H(\cdot)$) can be modeled by a Hill function that captures mRNA transcription, translation, and protein maturation.

5. The function governing GFP production includes basal production that captures both basal activation of P_{TET} and basal activation of $\text{P}_{TR-SSRE}$.

6. Mass conservation on the total concentration of $\text{P}_{TR-SSRE}$ sites ($p_T = p + C_m$) where p_T as the total concentration of $\text{P}_{TR-SSRE}$ sites.

7. Load due to $\text{P}_{TR-SSRE}$ promoter sites (4 SKN7 binding sites) for the GFP reporter is negligible compared to load of the $\text{P}_{TR-SSER}$ promoter sites in the 1x, 2x load plasmids (400, 800 SKN7 binding sites respectively).

Defining X_m as SKN7m and G_m as GFP, this leads to the following equations:

$$\dot{X}_m = k_m \frac{(DOX)^{n_1}}{K_{dox} + (DOX)^{n_1}} - \delta_X X_m \overbrace{-k_{on} X_m (p_T - C_m) + k_{off} C_m}^{s} \tag{U1}$$

$$\dot{C}_m = k_{on} X_m (p_T - C_m) - k_{off} C_m \tag{U2}$$

$$\dot{G}_m = k_{sgfp} + k_g \frac{(X_m)^{n_2}}{K_{gfp} + (X_m)^{n_2}} - \delta_G G_m \tag{U3}$$

where k_m and k_g are maximum activated protein production rates, $n1$ and $n2$ are hill coefficients, and K_{dox} and K_{gfp} are respective K_d for the hill functions, k_{sgfp} is the basal rate of GFP expression and all other rate parameters are as defined in the corresponding reactions. Note that s indicated in the equations represents the retroactivity flux in the $SKN7m$ dynamics.

Insulated system

The reactions considered for the insulated system are the DOX activated production of STAT5-HKRR from P_{TET}, the phosphorylation/dephospohrylation of STAT5-HKRR, STAT5-SNL1/YPD1/SKN7 phosphotransfer reactions, the SKN7 activated production of GFP, dephosphorylation reactions due to phosphatase (YPD1, single phosphorylated SKN7, double phosphorylated SKN7), and degradation/dilution of both STAT5-HKRR and GFP. Using the asterisk nonation (* or **) to denote single or double phosphorylation of species and C as the complex formed between SKN7 and $P_{TR-SSRE}$ (C* and C** correspond to SKN7 phosphorylation state), the reactions can be described by:

$$\phi \xrightarrow{f_H(DOX)} \text{STAT5-HKRR} \tag{2.6}$$

$$\text{STAT5-HKRR} \underset{k'_p}{\overset{k_p}{\rightleftharpoons}} \text{STAT5-HKRR}^* \tag{2.7}$$

$$\text{STAT5-HKRR}^* \xrightarrow{\delta} \phi \tag{2.8}$$

$$\text{STAT5-HKRR} \xrightarrow{\delta} \phi \tag{2.9}$$

$$\text{STAT5-HKRR}^* + \text{YPD1} \underset{k_2}{\overset{k_1}{\rightleftharpoons}} \text{STAT5-HKRR} + \text{YPD1}^* \tag{2.10}$$

$$\tag{2.11}$$

$$\text{SKN7+YPD1}^* \underset{k_4}{\overset{k_3}{\rightleftharpoons}} \text{SKN7}^*\text{+YPD1} \tag{2.12}$$

$$\text{SKN7}^*\text{+YPD1}^* \underset{k_4}{\overset{k_3}{\rightleftharpoons}} \text{SKN7}^{**}\text{+YPD1} \tag{2.13}$$

$$\text{SKN7}^* \xrightarrow{k_5} \text{SKN7} \tag{2.14}$$

$$\text{SKN7}^{**} \xrightarrow{k_6} \text{SKN7}^* \tag{2.15}$$

$$\text{YPD1}^* \xrightarrow{k_7} \text{YPD1} \tag{2.16}$$

$$\tag{2.17}$$

$$\mathrm{SKN7^{**} + p} \underset{k_{off}}{\overset{k_{on}}{\rightleftharpoons}} \mathrm{C^{**}} \tag{2.18}$$

$$\mathrm{SKN7^{*} + p} \underset{k_{off}}{\overset{k_{on}}{\rightleftharpoons}} \mathrm{C^{*}} \tag{2.19}$$

$$\mathrm{C^{**}} \xrightarrow{k_8} \mathrm{C^{*}} \tag{2.20}$$

$$\mathrm{C^{*}{+}YPD1^{*}} \underset{k_{10}}{\overset{k_9}{\rightleftharpoons}} \mathrm{C^{**}{+}YPD1} \tag{2.21}$$

$$\mathrm{C^{*}} \xrightarrow{k_{11}} \mathrm{SKN7 + p} \tag{2.22}$$

$$\mathrm{C^{*} + YPD1} \xrightarrow{k_{12}} \mathrm{YPD1^{*} + SKN7 + p} \tag{2.23}$$

$$\phi \xrightarrow{f_H(X^{**})} \mathrm{GFP} \tag{2.24}$$

$$\mathrm{GFP} \xrightarrow{\delta_g} \phi \tag{2.25}$$

For these reactions and the formation of subsequent ODEs, the following assumptions were made:

1. Reactions occur in single well-mixed compartment.

2. Extracellular DOX is in saturating conditions and there is rapid equilibrium between cytoplasm and extracellular media.

3. The functions governing production of STAT5-HKRR and GFP (denoted $f_H(\cdot)$) can be modeled by a Hill function that captures mRNA transcription, translation, and protein maturation.

4. STAT5-HKRR activation by JH1, phosphotransfer, and dimerization reactions can be modeled using a pseudo first order reaction that lump all intermediate processes together[15].

5. YPD1 and SKN7 are endogenously produced and their total concentration can be considered conserved ($SKN7_T = SKN7 + SKN7^{*} + SKN7^{**} + C^{*} + C^{**}$, $YPD1_T = YPD1 + YPD1^{*}$) [15].

6. SKN7 does not dimerize.[14].

7. SKN7 binds to $P_{TR-SSRE}$ only if D427 is phosphorylated to yield SKN7* due to a conformational change that allows the DNA binding domain to interact[13, 14].

8. SKN7* and SKN7** when bound to DNA to form C* and C** can still react with phosphatases and YPD1[14].

9. YPD1* reacts with SKN7* and SKN7** with same rates.

10. The function governing GFP production includes basal production that captures both basal activation of P_{TET} and basal activation of $P_{TR-SSRE}$.

11. Mass conservation on the total concentration of $P_{TR-SSRE}$ sites ($p_T = p + C^* + C^{**}$) where p_T as the total concentration of $P_{TR-SSRE}$ sites.

12. Load due to $P_{TR-SSRE}$ promoter sites (4 SKN7 binding sites) for the GFP reporter is negligible compared to load of the $P_{TR-SSER}$ promoter sites in the 1x, 2x load plasmids (400, 800 SKN7 binding sites respectively).

Defining Z as the STAT5-HKRR fusion, W as YPD1, X as SKN7, G as GFP and using the asterisk notation (*) to denote phosphorylation, these lead to the following equations:

$$\dot{Z} = k_m \frac{(DOX)^{n_1}}{K_{dox} + (DOX)^{n_1}} - \delta Z - k_2 W^* Z + k_1 Z^* (W_T - W^*) - k_p Z + k_p' Z^* \tag{I1}$$

$$\dot{Z}^* = -k_1 Z^* (W_T - W^*) + k_2 W^* Z + k_p Z - k_p' Z^* - \delta Z^* \tag{I2}$$

$$\begin{aligned}\dot{W}^* =& k_1 Z^* (W_T - W^*) - k_2 W^* Z - k_3 \left(X_T - X^* - X^{**} \boxed{-C^* - C^{**}} \right) W^* \\ &+ k_4 X^* (W_T - W^*) - k_3 X^* W^* + k_4 X^{**} (W_T - W^*) - k_7 W^* \\ &\overbrace{-k_9 C^* W^* + k_{10} C^{**} (W_T - W^*) + k_{12} (W_T - W^*) C^*}^{s_1}\end{aligned} \tag{I3}$$

$$\begin{aligned}\dot{X}^* =& k_3 \left(X_T - X^* - X^{**} \boxed{-C^* - C^{**}} \right) W^* - k_4 X^* (W_T - W^*) - k_3 X^* W^* \\ &+ k_4 X^{**} (W_T - W^*) - k_5 X^* + k_6 X^{**} \overbrace{-k_{on} X^* (p_T - C^* - C^{**}) + k_{off} C^*}^{s_2}\end{aligned} \tag{I4}$$

$$\dot{X}^{**} = k_3 X^* W^* - k_4 X^{**} (W_T - W^*) - k_6 X^{**} \overbrace{-k_{on} X^{**} (p_T - C^* - C^{**}) + k_{off} C^{**}}^{s_3} \tag{I5}$$

$$\begin{aligned}\dot{C}^* =& k_{on2} X^* (p_T - C^* - C^{**}) - k_{off} C^* + k_8 C^{**} - k_9 C^* W^* + k_{10} C^{**} (W_T - W^*) \\ &- k_{11} C^* - k_{12} (W_T - W^*) C^*\end{aligned} \tag{I6}$$

$$\dot{C}^{**} = k_{on}X^{**}(p_T - C^* - C^{**}) - k_{off}C^{**} - k_8C^{**} + k_9C^*W^* - k_{10}C^{**}(W_T - W^*) \quad \text{(I7)}$$

$$\dot{G} = k_{sgfp} + k_g\frac{(X^{**})^{n_2}}{K_{gfp} + (X^{**})^{n_2}} - \delta_G G \quad \text{(I8)}$$

where k_m and k_g are maximum activated protein production rates, $n1$ and $n2$ are hill coefficients, and K_{dox} and K_{gfp} are respective K_d for the hill functions, k_{sgfp} is the basal rate of GFP expression and all other rate parameters are as defined in the corresponding reactions.The terms under braces s_i represent the retroactivity fluxes and the boxed terms affect directly the availability of SKN7.

Parameters

Constraints

Because both circuits have the same P_{TET} promoter driving SKN7m and STAT5-HKRR respectively and SKN7m, SKN7* , SKN7** have the same binding domain for activation of $P_{TR-SSRE}$, we assume the same Hill function (parameters k_m, k_g, $n1$, $n2$, K_{dox}, and K_{gfp}) for both the uninsulated and insulated circuits. Additionally, because SKN7m, SKN7* , SKN7** have the same binding domain, we assume the same k_{on} and k_{off} rate constants. These assumptions are not crucial to the objective of this study (insulation device design and analysis), but reduce the number of parameters and help simplify the model.

To examine only biologically relevant parameter sets in all systems, we constrained each parameter prior to meeting based on literature references:

1. δ_G and δ_X were constrained by both the doubling time observed experimentally (180min) and average half-life of a yeast protein (43 min)[10] due to both STAT5-HKRR and GFP being without degradation tags and no known targeted degradation machinery.

2. K_{dox} was constrained by the dosage-response curve to fall between 1nM and 20μM.

3. K_{gfp} was constrained to be between 1nM and 10nM based on prior calculated K_D for a variety of strong yeast promoters [16].

4. k_m and k_g were constrained in the following manner. Because the $P_{TR-SSRE}$ and P_{TET} promoters are MEL1 and CYC1 derivatives, it is expected they would drive transcription/translation to similar steady-state levels of proteins in yeast, 0.001 - 30 μM[17]. Thus, we utilized the ratio between production and degradation (k_m / δ) set equal to the average protein concentration to obtain the parameters.

5. $n1$ and $n2$ were thought to be ≥ 1 but left unconstrained during fitting.

6. k_1, k_2, k_3, and k_4 were constrained to fall between 1 μM s^{-1} and 50 μM s^{-1} based on *in vitro* experiments[11] and prior modeling studies[15]. Additionally, because it is known that SKN7 is a weaker acceptor and donor of phosphates than YPD1[11], we made use of the following relations: $k_1 \geq k_3$ and $k_2 \geq k_4$.

7. k_p, k'_p, k_5, k_6, k_7, k_8 were constrained to fall between 0.004 - 1 min^{-1} based on ranges of phosphorylation rates found in prior modeling studies[15, 18].

8. k_9, k_{10}, and k_{12} were constrained by the following relations: $k_9 \leq k_3$, $k_{10} \leq k_4$, and $k_{12} \leq k_4$ due to the DNA preventing YPD1 access to bound SKN7 species (steric hindrance[19]).

9. k_{11} was unconstrained during fits but thought to be $\leq$ 1 min^{-1} as it governs a rare event (activated, conformationally stabilized protein dephosphorylating and subsequently unbinding).

10. k_{on} was bounded in the 10^5 - 10^6 $[M\ sec]^{-1}$ range governing most protein-protein associations[20].

11. k_{off} was bounded in conjunction with k_{on} via constraining the K_D to be between 0.01nM and 10μM. This range covers covers protein-DNA half lives between tens of minutes to subseconds as well as includes known transcriptional regulators (0.1 nM for Zif268, a very strong Zinc-finger binding protein to GCGTGGCGC[21] and 0.3 μM for dHax3 a TAL effector that binds TCCCTTTATCTCT)[22].

12. p_T was calculated by taking the total sum of $P_{TR-SSRE}$ promoters (800 on the 2μ) and dividing by the yeast cell volume (60e-15 L)[23].

13. $SKN7_{TOT}$ and $YPD1_{TOT}$ were calculated by taking the endogenous amounts in the YeastGFP Localization Database[17] and dividing by the yeast cell volume[23].

As we can see from Figure 2-3 (a)-(c), GFP of the unloaded uninsulated system (Model) has the same trajectory as the loaded uninsulated system with the 4 promoter sites included in the genome (Model + 0x). The GFP trajectory of the loaded uninsulated system with 800 promoter sites (Model + 2x) shows a significant lag and attenuation due to load, relative to the unloaded uninsulated system. These justify assumption 7 of the uninsulated system and assumption 12 of the insulated system. The time varying inputs were chosen in order to maximize the steady state peak to peak amplitude percent error between the loaded and unloaded trajectory of GFP. In order to determine what input profiles would lead to the largest effects, we simulated system U1-U3 for a range of time varying inputs with square-wave shape and calculating the error percent:

$$\%Error = \frac{\text{Amp}[GFP(t)] - \text{Amp}[G_{mL}(t)]}{\text{Amp}[GFP(t)]}.$$

Here $\text{Amp}[X(t)]$ denotes the peak to peak amplitude of oscillation of $X(t)$, defined as

$$\text{Amp}[X(t)] = \max[X(t)] - \min[X(t)] \text{ for } t > t_0$$

where t_0 denotes the time when $X(t)$ reaches its steady state response. The uninsulated system was simulated for square wave inputs where the width and period of the square wave were varied to determine the range of period/width that provided the greatest retroactivity effect. The results are shown in Figure 2-4 where the heat map depicts the percentage error for the given period/width input. From the figure we concluded that the system would show the largest amplitude difference for a square wave profile of small width and high period, thus the dynamic experiments were carried out for square wave DOX inputs with a width of 50min for the periods: 150min,

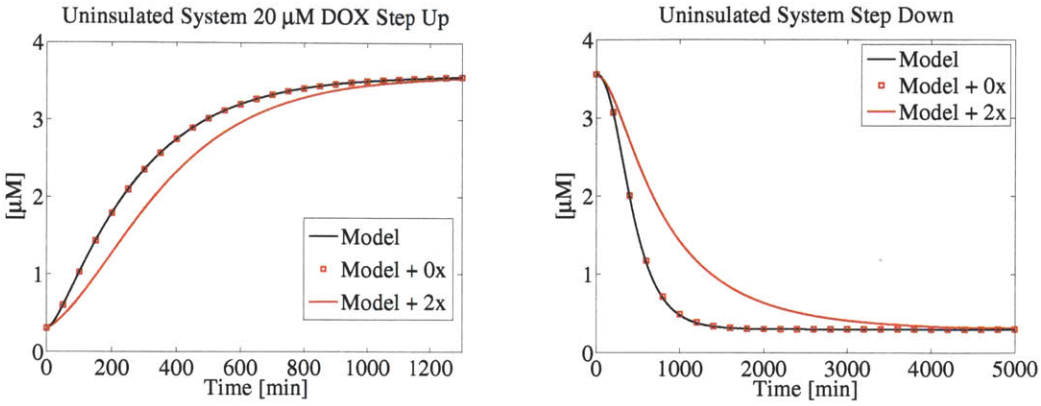

(a) Step up experiment

(b) Step down experiment

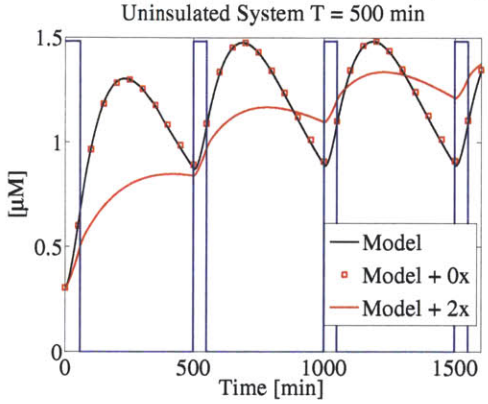

(c) Dynamic input, T = 500 [min]

Figure 2-3: Uninsulated system GFP trajectory simulations using the initial parameter set. The panels present the GFP trajectory of the uninsulated system U1-U3 for the step up (a) using 20 μM DOX, step down (b) and period T = 500 [min], experiments (c). The isolated system (Model) has the same response as the system accouting for the 4 chromosomally integrated $P_{TR-SSRE}$ promoter sites (Model +0x). The GFP trajectory subjected to the high copy number plasmid $P_{TR-SSRE}$ promoter sites is given by (Model + 2x). With this simulation it was concluded, that the chromosomally integrated promoter sites had negligible effects on the GFP dynamics, thus justifying the uninsulated system assumption 7 and the insulated system assumption 12.

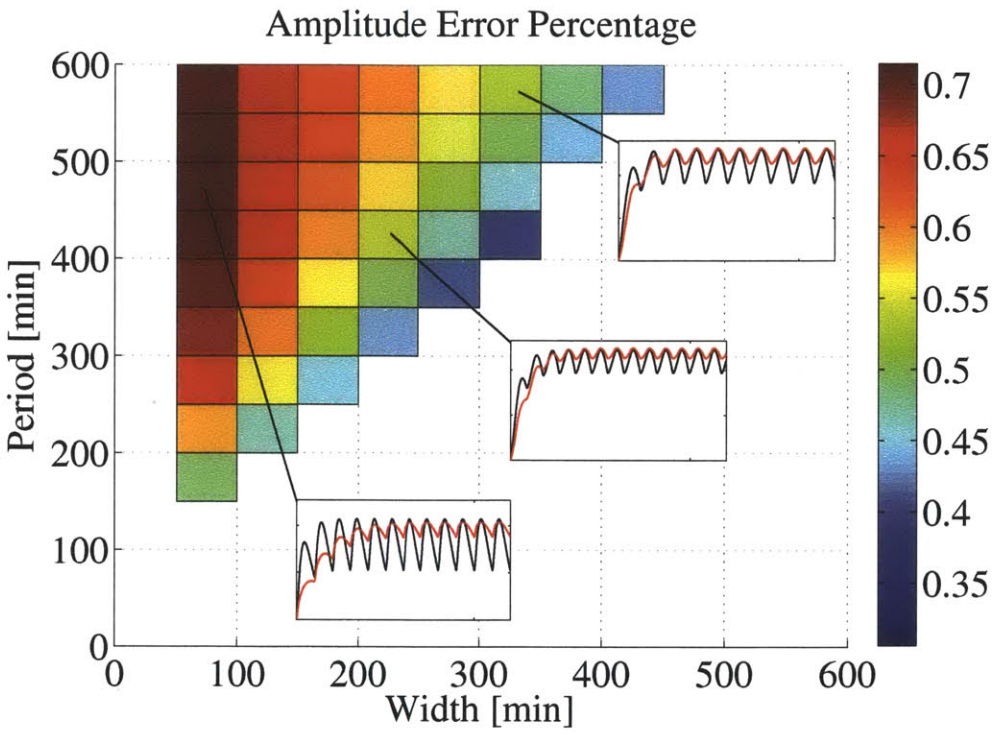

Figure 2-4: Peak to peak output error heat map for the dynamic experiment design. System U1-U3 was simulated using the Table B-1 initial parameter set to determine the input profile maximizing the amplitude attenuation retroactivity effect on the uninsulated system. It was determined that DOX inputs of 50 min width for various induction periods would provide the greatest retroactivity effects for the validation of the insulation device design.

200min, 250min, 350min and 500min. The data from these experiments was used to improve the fit and the updated kinetic parameters are given in the "Final Fit" columns of Table B-1 & Table B-2, where all values are inside their physical range. The parameters provided in the "Final Fit" columns of Table B-1 & Table B-2 are the ones used for the rest of the analysis.

2.1.3 Mathematical explanation of the insulation device

This section illustrates how the ODE model in equations I1-I8 fits the structure of the class of systems to which the result of Jayanthi *et. al* applies [8]. In particular,it is explicitly shown how this structure enables attenuation of the effect of retroactivity fluxes $s_1 = -k_9 C^* W^* + k_{10} C^{**}(W_T - W^*) + k_{12}(W_T - W^*)C^*$, $s_2 = -k_{on} X^*(p_T - C^* - C^{**}) + k_{off} C^*$ and $s_3 = -k_{on} X^{**}(p_T - C^* - C^{**}) + k_{off} C^{**}$ on the insulation device dynamics. Finally, an intuitive interpretation of the result in terms of fluxes controlling X^{**} is provided. Let $Z_T := Z + Z^*$ and re-write system I1-I8 by replacing Z with Z_T:

$$\dot{Z}_T = k_m \frac{(DOX)^{n1}}{K_{dox} + (DOX)^{n1}} - \delta Z_T \tag{2.26}$$

$$\dot{Z}^* = -k_1 Z^*(W_T - W^*) + k_2 W^*(Z_T - Z^*) + k_p(Z_T - Z^*) - k_p' Z^* - \delta Z^* \tag{2.27}$$

$$\begin{aligned}\dot{W}^* =& k_1 Z^*(W_T - W^*) - k_2 W^*(Z_T - Z^*) - k_3(X_T - X^* - X^{**} - C^* - C^{**})W^* \\ &+ k_4 X^*(W_T - W^*) - k_3 X^* W^* + k_4 X^{**}(W_T - W^*) - k_7 W^* \\ &- k_9 C^* W^* + k_{10} C^{**}(W_T - W^*) + k_{12}(W_T - W^*)C^*\end{aligned} \tag{2.28}$$

$$\begin{aligned}\dot{X}^* =& k_3(X_T - X^* - X^{**} - C^* - C^{**})W^* - k_4 X^*(W_T - W^*) - k_3 X^* W^* \\ &+ k_4 X^{**}(W_T - W^*) - k_5 X^* + k_6 X^{**} - k_{on} X^*(p_T - C^* - C^{**}) + k_{off} C^*\end{aligned} \tag{2.29}$$

$$\dot{X}^{**} = k_3 X^* W^* - k_4 X^{**}(W_T - W^*) - k_6 X^{**} - k_{on} X^{**}(p_T - C^* - C^{**}) + k_{off} C^{**} \tag{2.30}$$

$$\begin{aligned}\dot{C}^* =& k_{on} X^*(p_T - C^* - C^{**}) - k_{off} C^* + k_8 C^{**} - k_9 C^* W^* + k_{10} C^{**}(W_T - W^*) \\ &- k_{11} C^* - k_{12}(W_T - W^*)C^*\end{aligned} \tag{2.31}$$

$$\dot{C}^{**} = k_{on} X^{**}(p_T - C^* - C^{**}) - k_{off} C^{**} - k_8 C^{**} + k_9 C^* W^* - k_{10} C^{**}(W_T - W^*), \tag{2.32}$$

in which the G dynamics were neglected, which are not relevant for the current analysis as they do not affect the dynamics of X^{**}, the output of the insulation

device. The concentrations were normalized by their maximum values, that is, the non-dimensional concentrations were defined as

$$x^* := \frac{X^*}{X_T}, \quad x^{**} := \frac{X^{**}}{X_T}, \quad w^* := \frac{W^*}{W_T}, \quad z_T := \frac{Z_T}{Z_0}, \quad z^* := \frac{Z^*}{Z_0}, \quad c^* := \frac{C^*}{p_T}, \quad c^{**} := \frac{C^{**}}{p_T},$$

in which Z_0 is the maximal value reachable by Z_T given by $Z_0 := k_m/\delta$. System (2.26)-(2.32) in the non-dimensional variables becomes

$$\dot{z}_T = \delta \frac{(DOX)^{n1}}{K_{dox} + (DOX)^{n1}} - \delta z_T \tag{2.33}$$

$$\dot{z}^* = -k_1 W_T z^*(1-w^*) + k_2 W_T w^*(z_T - z^*) + k_p(z_T - z^*) - k_p' z^* - \delta z^* \tag{2.34}$$

$$\begin{aligned}\dot{w}^* =& k_1 Z_0 z^*(1-w^*) - k_2 Z_0 w^*(z_T - z^*) - k_3 X_T \left[1 - x^* - x^{**} - \frac{p_T}{X_T}(c^* - c^{**})\right] w^* \\ &+ k_4 X_T x^*(1-w^*) - k_3 X_T x^* w^* + k_4 X_T x^{**}(1-w^*) - k_7 w^* \\ &- k_9 p_T c^* w^* + k_{10} p_T c^{**}(1-w^*) + k_{12} p_T c^*(1-w^*)\end{aligned} \tag{2.35}$$

$$\begin{aligned}\dot{x}^* =& k_3 X_T \left[1 - x^* - x^{**} - \frac{p_T}{X_T}(c^* - c^{**})\right] w^* - k_4 W_T x^*(1-w^*) - k_3 W_T x^* w^* \\ &+ k_4 W_T x^{**}(1-w^*) - k_5 x^* + k_6 x^{**} - k_{on} p_T x^*(1 - c^* - c^{**}) + k_{off} \frac{p_T}{X_T} c^*\end{aligned} \tag{2.36}$$

$$\begin{aligned}\dot{x}^{**} =& k_3 W_T x^* w^* - k_4 W_T x^{**}(1-w^*) - k_6 x^{**} - k_{on} p_T x^{**}(1 - c^* - c^{**}) \\ &+ k_{off} \frac{p_T}{X_T} c^{**}\end{aligned} \tag{2.37}$$

$$\begin{aligned}\dot{c}^* =& k_{on} X_T x^*(1 - c^* - c^{**}) - k_{off} c^* + k_8 c^{**} - k_9 W_T c^* w^* + k_{10} W_T c^{**}(1-w^*) \\ &- k_{11} c^* - k_{12} W_T (1-w^*) c^*\end{aligned} \tag{2.38}$$

$$\dot{c}^{**} = k_{on} X_T x^{**}(1 - c^* - c^{**}) - k_{off} c^{**} - k_8 c^{**} + k_9 W_T c^* w^* - k_{10} W_T c^{**}(1-w^*). \tag{2.39}$$

While the time scale of the first differential equation is determined by the dilution rate $\delta \in [0.004, 0.01]$ min^{-1} the timescale of the remaining differential equations is much faster and determined by phosphotransfer reactions. Specifically, we can consider the reactions involving kinetic rates $\{k_p,\ k_1,\ k_2,\ k_3,\ k_4,\ k_6\}$ as evolving in a fast timescale characterized by the phosphorylation rate $k_4 W_T \in [6, 600]$ min^{-1} (see Table B-2 final fit set). Based on the parameters in Table B-2 final fit set, the remaining phosphotransfer reactions, including spontaneous dephosphorylation of x^* and w^* as well as phosphotransfer reactions of the protein/DNA complex, evolve in a slower time scale since $\{k_5,\ k_7,\ k_8,\ k_9 p_T, k_{10} p_T,\ k_{11},\ k_{12} p_T\} \leq 0.02$ min^{-1}. Furthermore, the

binding/unbinding of x^* and x^{**} with DNA occurs at a maximum rate $k_{on}p_T \leq 0.13$ min^{-1}. Thus, we can justify the application of singular perturbation theory with small parameter $\epsilon = \delta/(k_4 W_T)$, in particular with constants not depending on ϵ: $c_1 := k_1/k_4$, $c_2 := k_2/k_4$, $c_3 := k_3/k_4$, $c_5 := k_5/\delta$ $c_6 := k_6/(k_4 W_T)$, $c_7 := k_7/\delta$, $c_8 := k_8/\delta$, $c_9 := k_9 p_T/\delta$, $c_{10} := k_{10}p_T/\delta$, $c_{11} := k_{11}/\delta$, $c_{12} := k_{12}p_T/\delta$, $\kappa_p := k_p/(k_4 W_T)$, $\kappa_p' := k_p'/\delta$, $\alpha := X_T/W_T$, $\kappa_{on} := k_{on}p_T/\delta$, and $\kappa_{off} := k_{off}(p_T/X_T)/\delta$. Then, system (2.33)-(2.39) becomes

$$\dot{z}_T = \delta \frac{(DOX)^{n1}}{K_{dox} + (DOX)^{n1}} - \delta z_T \tag{2.40}$$

$$\epsilon \dot{z}^* = -c_1 \delta z^*(1-w^*) + c_2 \delta w^*(z_T - z^*) + \kappa_p \delta (z_T - z^*) - \epsilon \kappa_p' \delta z^* - \epsilon \delta z^* \tag{2.41}$$

$$\begin{aligned}\epsilon \dot{w}^* =& c_1 \delta (Z_0/W_T) z^*(1-w^*) - c_2 \delta (Z_0/W_T) w^*(z_T - z^*) + \alpha \delta x^*(1-w^*) \\ & - c_3 \alpha \delta x^* w^* - c_3 \alpha \delta \left(1 - x^* - x^{**} \boxed{-(p_T/X_T)c^* - (p_T/X_T)c^{**}}\right) w^* \\ & + \alpha \delta x^{**}(1-w^*) - \epsilon c_7 \delta w^* \overbrace{+\epsilon c_9 \delta c^* w^* + \epsilon c_{10} \delta c^{**}(1-w^*) + \epsilon c_{12} \delta c^*(1-w^*)}^{\bar{s}_1}\end{aligned} \tag{2.42}$$

$$\begin{aligned}\epsilon \dot{x}^* =& c_3 \delta \left(1 - x^* - x^{**} \boxed{-(p_T/X_T)c^* - (p_T/X_T)c^{**}}\right) w^* - \delta x^*(1-w^*) - c_3 \delta x^* w^* \\ & + \delta x^{**}(1-w^*) + c_6 \delta x^{**} - \epsilon c_5 \delta x^* \overbrace{-\epsilon \kappa_{on} \delta x^*(1 - c^* - c^{**}) + \epsilon \kappa_{off} \delta c^*}^{\bar{s}_2}\end{aligned} \tag{2.43}$$

$$\epsilon \dot{x}^{**} = c_3 \delta x^* w^* - c_6 \delta x^{**} - \delta x^{**}(1-w^*) \overbrace{-\epsilon \kappa_{on} \delta x^{**}(1 - c^* - c^{**}) + \epsilon \kappa_{off} \delta c^{**}}^{\bar{s}_3} \tag{2.44}$$

$$\begin{aligned}\dot{c}^* =& \kappa_{on} \delta (X_T/p_T) x^*(1 - c^* - c^{**}) - \kappa_{off} \delta (p_T/X_T) c^* + c_8 \delta c^{**} - c_9 \delta (W_T/p_T) c^* w^* \\ & + c_{10} \delta (W_T/p_T) c^{**}(1-w^*) - c_{11} \delta c^* - c_{12} \delta (W_T/p_T)(1-w^*) c^*\end{aligned} \tag{2.45}$$

$$\begin{aligned}\dot{c}^{**} =& \kappa_{on} \delta (X_T/p_T) x^{**}(1 - c^* - c^{**}) - \kappa_{off} \delta (X_T/p_T) c^{**} - c_8 \delta c^{**} \\ & + c_9 \delta (W_T/p_T) c^* w^* - c_{10} \delta (W_T/p_T) c^{**}(1-w^*).\end{aligned} \tag{2.46}$$

Since $\epsilon \ll 1$, the above system is well approximated by a reduced system where $\epsilon = 0$. The trajectories of the above system approach those of the reduced system very fast when ϵ is very small and when the slow manifold, obtained setting $\epsilon = 0$ in equations (2.41)-(2.44), is locally exponentially stable. In such a case, note that the fluxes under brace $\bar{s}_1$, $\bar{s}_2$ and $\bar{s}_3$ become zero, so that the dynamics of the insulation device, that is, of (z^*, w^*, x^*, x^{**}) are not appreciably affected by the load unless $(p_T/X_T)(c^* + c^{**})$ in (2.42) and (2.43) is comparable to 1. We have that $(p_T/X_T)(c^* + c^{**}) \ll 1$ if $p_T \ll X_T$ since $c^*, c^{**} < 1$. From the parameters in Table B-1 & Table B-2 final fit set, we have

that $p_T/X_T \approx 0.28$. Defining $k_d := k_{off}/k_{on}$ we have that $c^* < X_T x^*/(X_T + k_d)$ and $c^{**} < X_T x^{**}/(X_T + k_d)$ at the quasi-steady state. Furthermore, assuming the maximum activation of x^* and x^{**} stays bellow 30% of its total concentration (small signal assumption), based on the values of Table B-1 & Table B-2 final fit set, we obtain that $c^*, c^{**} < 0.29$, leading to having $(p_T/X_T)(c^* + c^{**})$ to be about 0.17. Since $c = 0$ initially, we have that retroactivity will have no appreciable effect during the transient and will manifest itself with a small steady state error. This steady state error will be smaller as p_T/X_T becomes smaller, which can be obtained by increasing X_T in the insulated system. The loaded insulated system experimental data (pending publication) and simulation results for the nominal parameter values show that the residual steady state error due to retroactivity is barely appreciable for the parameter set. Hence, this term is neglected in the following treatment assuming that X_T is large enough so that p_T/X_T is small.

In order to claim that the trajectories of system (2.40)-(2.46) approach fast those of the reduced system where $\epsilon = 0$, we need to have that the slow manifold is locally exponentially stable [9]. This is checked by verifying that the Jacobian of the fast system with $\epsilon = 0$:

$$\dot{z}^* = -c_1 z^*(1 - w^*) + c_2 w^*(z_T - z^*) + \kappa_p(z_T - z^*) \tag{2.47}$$

$$\begin{aligned}\dot{w}^* =& c_1(Z_0/W_T)z^*(1 - w^*) - c_2(Z_0/W_T)w^*(z_T - z^*) - c_3\alpha(1 - x^* - x^{**})w^* \\ &+ \alpha x^*(1 - w^*) - c_3\alpha x^* w^* + \alpha x^{**}(1 - w^*)\end{aligned} \tag{2.48}$$

$$\dot{x}^* = c_3(1 - x^* - x^{**})w^* - x^*(1 - w^*) - c_3 x^* w^* + x^{**}(1 - w^*) + c_6 x^{**} \tag{2.49}$$

$$\dot{x}^{**} = c_3 x^* w^* - x^{**}(1 - w^*) - c_6 x^{**} \tag{2.50}$$

has eigenvalues with strictly negative real parts uniformly in z_T when (z^*, w^*, x^*, x^{**}) are on the slow manifold ($\epsilon = 0$ in equations (2.41)-(2.44)). This Jacobian is given by

$$J = \begin{bmatrix} -c_1(1 - w^*) - c_2 w^* & c_1 z^* + c_2(z_T - z^*) & 0 & 0 \\ A & B & +\alpha(1 - w^*) & c_3\alpha w^* + \alpha(1 - w^*) \\ 0 & C & -2c_3 w^* - (1 - w^*) & -c_3 w^* + (1 - w^*) + c_6 \\ 0 & c_3 x^* + x^{**} & c_3 w^* & -(1 - w^*) - c_6 \end{bmatrix}$$

in which

$$A = c_1(Z_0/W_T)(1 - w^*) + c_2(Z_0/W_T)w^*,$$

$$B = -c_1(Z_0/W_T)z^* - c_2(Z_0/W_T)(z_T - z^*) - c_3\alpha(1 - x^* - x^{**}) - \alpha x^* - c_3\alpha x^* - \alpha x^{**},$$

$$C = c_3(1 - x^* - x^{**}) + x^* - c_3x^* - x^{**}.$$

The Jacobian of the system was numerically calculated as a function of z_T and verified that the eigenvalues have strictly negative real part as seen in Figure 2-5, where the largest eigenvalue is bounded between -0.003 and -0.025.

2.1.4 Qualitative explanation of the insulation device

Consider the ODE model (2.40)-(2.46) and let $u(t) := \frac{DOX(t)^{n_1}}{K_{dox}+DOX(t)^{n_1}}$. At the quasi-steady state ($\epsilon = 0$), we have that all the insulated circuit species are static functions of $u(t)$. Re-write the differential equation of $x^{**}(t)$ in (2.44) letting $G := 1/\epsilon$ and multiplying both sides by X_T, so that

$$\dot{X}^{**} = c_3G\delta X^*w^*(u(t)) - \delta GX^{**}(1 - w^*(u(t))) - c_6G\delta X^{**} - \kappa_{on}\delta X^{**}(1 - c^* - c^{**}) + \kappa_{off}X_T\delta c^{**}.$$

Letting $\hat{s}_3 = \kappa_{on}\delta X^{**}(1 - c^* - c^{**}) + \kappa_{off}X_T\delta c^{**}$, and recalling the expressions of G, c_3 and c_6 from Section 2.1.3, we define

$$G_1 := c_3G\delta X_T = k_3W_TX_T,\ G_2 := \delta G = k_4W_T,$$

$F_1(u(t)) := w^*(u(t))x^*(u(t))$ and $F_2(u(t)) = (c_6 + (1 - w^*(u(t)))$, so that

$$\dot{X}^{**} = G_1F_1(u(t)) - G_2F_2(u(t))X^{**} - \hat{s}_3.$$

Note that $F_1(u(t))$ and $F_2(u(t))$ do not depend on the load by virtue of the assumption that p_T/X_T is sufficiently small and by the fact that $\bar{s}_1 = \bar{s}_2 = 0$ in equation (2.42)-(2.43) when $\epsilon = 0$. At the quasi-steady state, the inlet and outlet fluxes determining

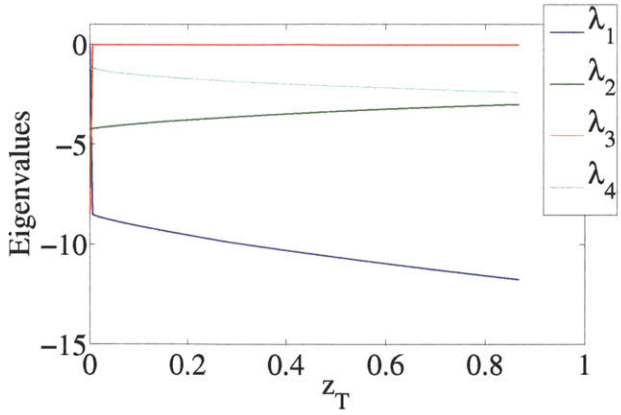

Figure 2-5: Load drivers reduced order system eigenvalues at different normalized STAT5 concentrations. The Jacobian of system (2.47)-(2.50) was numerically calculated for varying normalized z_T concentrations. The systems eigenvalues have strictly negative parts, with the slowest eigenvalue bounded between -0.003 and -0.025.

the rate of change of X^{**} balance out, so that

$$G_1F_1(u(t)) - G_2F_2(u(t))X^{**} - \hat{s}_3 = 0,$$

leading to

$$X^{**} = X_T\left(\frac{k_3}{k_4}\frac{F_1(u(t))}{F_2(u(t))} - \frac{\hat{s}_3}{k_4X_TW_TF_2(u(t))}\right). \tag{2.51}$$

From these expressions, it follows that if $k_4X_TW_T \gg \hat{s}_3$, then the dynamic behavior of $X^{**}(t)$ is not affected by retroactivity flux $\hat{s}_3$. Since the phosphorylation reactions are very fast compared to the other reactions in the system (as seen in Table B-2 final fit set), the fluxes due to the phosphorylation reactions $G_1F_1(u(t))$ and $G_2F_2(u(t))$ are much larger than the retroactivity flux $\hat{s}_3$. Therefore $k_4X_TW_T \gg \hat{s}_3$ holds.

2.2 Sensitivity Analysis

To single out specific parameters to which the retroactivity attenuation property is particularly sensitive, a sensitivity analysis is performed. Specifically, from the results of the two previous sections, it is clear that the retroactivity attenuation property is controlled by parameter ϵ. Since ϵ is small when the reactions involving the kinetic rates $\{k_p, k_1W_T, k_2W_T, k_3W_T, k_4W_T, k_6\}$ are in a timescale of order k_4W_T, much larger than δ, we expect that uniform decrease in these parameters will worsen retroactivity attenuation.

Observing that the nominal solution of the insulated system in I1-I8 has at least continuous first derivatives on the parameters not shared between the insulated and uninsulated systems, which we will denote as parameter the vector λ, we can define the sensitivity of a state trajectory $X(t,\lambda)$ to parameters λ by taking the partial derivative with respect to λ [*REF*[9]]:

$$S_\lambda(t,\lambda) = \frac{\partial}{\partial\lambda}X(t,\lambda), \tag{2.52}$$

which is a matrix in $\mathbb{R}^{nxp}$, where n is the number of states and p is the number of

parameters in λ. Now take the derivative with respect to time of the sensitivity to obtain

$$\begin{aligned}\frac{d}{dt}\left[\frac{\partial}{\partial\lambda}X(t,\lambda)\right] &= \frac{\partial}{\partial\lambda}\left[\frac{d}{dt}X(t,\lambda)\right] \\ &= \frac{\partial}{\partial\lambda}f(t,X(t,\lambda),\lambda) \\ &= \left.\frac{\partial f(t,X,\lambda)}{\partial X}\right|_{X=X(t,\lambda)}\frac{\partial}{\partial\lambda}X(t,\lambda) + \left.\frac{\partial f(t,X,\lambda)}{\partial\lambda}\right|_{X=X(t,\lambda)},\end{aligned}$$

and define the Jacobian matrices:

$$A(t,\lambda) := \left.\frac{\partial f(t,X,\lambda)}{\partial X}\right|_{X=X(t,\lambda)}, \quad B(t,\lambda) := \left.\frac{\partial f(t,X,\lambda)}{\partial\lambda}\right|_{X=X(t,\lambda)}.$$

From this, we can write the differential equation for the sensitivity matrix as

$$\dot{S}_\lambda = A(t,\lambda_0)S_\lambda(t) + B(t,\lambda_0), \tag{2.53}$$

where the Jacobian matrices A and B are evaluated at the nominal parameter values λ_0 . In our case we have $X = (Z,\ Z^*,\ W^*,\ X^*,\ X^{**},\ C^*,\ C^{**})^T$ and $\lambda = (\delta,\ k_p,\ k_p,\ k_1,\ k_2,\ k_3,\ k_4,\ k_5,\ k_6,\ k_7,\ X_T,\ W_T,\ k_8,\ k_9,\ k_{10},\ k_{on},\ k_{off},\ p_T,\ k_{11},\ k_{12})^T$ with λ_0 given in Table B-2 final fit set. Multiplying S_λ on the right hand side by the diagonal matrix $D_\lambda = \text{diag}\{\lambda_1, \lambda_2, \ldots, \lambda_n\}$, we can define the sensitivity as the concentration change of species X due to a percentile change in the individual parameter λ_i. We call $\bar{S}_\lambda = S_\lambda D_\lambda$ the normalized sensitivity, which allows for sensitivity comparison between parameters of different nature.

2.2.1 Unloaded insulated system dynamic sensitivity

The results for the dynamic sensitivity analysis of the unloaded insulated system for the T = 500 [min] experiment, observing only the sensitivity of state $X^{**}(t,\lambda)$, are given in Figure 2-6. In these plots, positive sensitivity value accounts for an increase in the overall amplitude of response while negative sensitivity value accounts for a decrease. Also, comparing the maximum amplitude of oscillation reached by all

parameters indicates which one has the largest weight on shaping the output response. If we look at the reaction rates in list (2.6) - (2.25), we see that the reactions in the forward phosphotransfer path leading to the formation of X^{**} (k_1, k_3 in Figure 2-6 (a)-(b)) have positive sensitivity. This means that a percentile increment in these parameters leads to an increase of the overall response. Phosphotransfer parameters in the backward path (k_2, k_4, k_5, k_6 in Figure 2-6(b)-(c)) have negative sensitivity, thus increasing them leads to a decrease in the response amplitude.

To interpret the higher sensitivity of X^{**} to parameters δ (decay of Z and Z^*) and k_p (phosphorylation of Z^*), as seen in Figure 2-6 (a), consider first how Z^* acts as an input to the reactions of the insulation device controlling the expression of X^{**}. From reaction (2.10), we see that Z^* acts as a kinase in the STAT5/YPD1 cycle, controlling the production of W^*. At the same time, from reaction (2.12) and (2.13) we see that W^* acts as a kinase in the YPD1/SKN7 cycle, controlling the production of X^{**}. Thus, in the phosphorylation cascade STAT5/YPD1/SKN7 (comprising the insulation device) we can visualize Z^* acting as the cascade input and X^{**} as the cascade output. Increasing the decay parameter δ leads to a decrease in the maximum Z^* concentration, resulting in a decrease of the maximum X^{**} concentration. Conversely, looking at reaction (2.7) we see that increasing the phosphorylation parameter k_p leads to an increase in the Z^* concentration, which results in an increase of the concentration of X^{**}. The system appears to be most sensitive to this parameter since k_p regulates the maximum concentration of the input that the insulation device sees.

2.2.2 Loaded insulated system dynamic sensitivity

The results for the sensitivity analysis of the loaded system, again only considering state X^{**}, are given in Figure 2-7. Here we see the same qualitative sensitivity behavior as in the unloaded case: parameters in the forward path have positive sensitivity while parameters in the backward path have negative sensitivity. The system is again more sensitive to parameters δ and k_p (Figure 2-7 (a)) at the input stage of the insulation device, interpreted as Section 2.2.1. It is also worth noting the increased

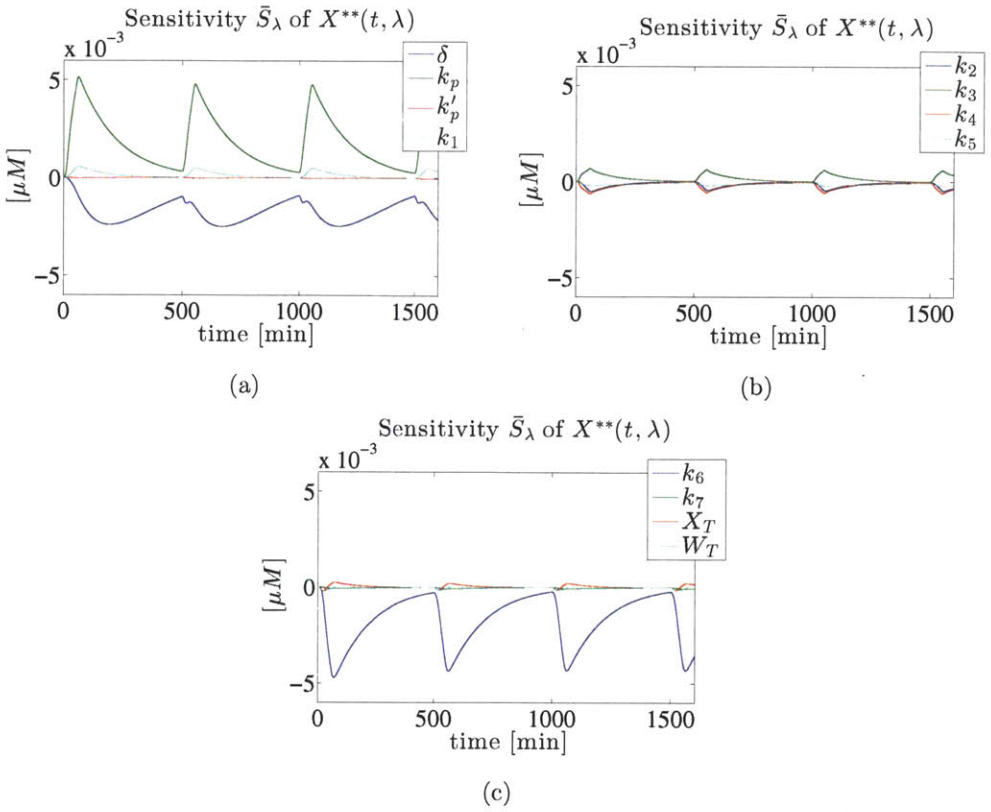

Figure 2-6: Dynamic sensitivity of the unloaded insulated system. The dynamic sensitivity given by (2.53) was calculated across all insulated system parameters with nominal parameters given in Table B-2 final fit set. The simulations present the normalized dynamic sensitivity given by multiplying the solution of (2.53) by the diagonal matrix D_λ containing all parameter values. The insulated system in isolation is most sensitive to parameters δ and k_p of the STAT5 reactions and the SKN7 dephosphorylation rate k_6. Percentage variations in these parameters results in a greater amplitude of oscillation change in the SKN7 output protein concentration.

sensitivity to W_T and X_T compared to the unloaded insulated system sensitivity, as it can be seen by comparing Figure 2-6 (c) with Figure 2-7 (c). This can be interpreted from a physical standpoint as follows. The increased sensitivity to X_T can be seen as the systems need for high substrate to supply the additional flux created by the interconnection with the downstream load component. To prevent dependence of the quasi-steady state of system I1-I8 from the load, the substrate needs to be in high abundance to meet the load demands. Additionally, since the complexes created with the load promoter sites undergo phosphotransfer reactions with W and W^*, the total YPD1 concentration W_T plays now a larger role than in the unloaded case in which these reactions were absent, as it can be seen in Figure 2-7 (c).

The X^{**} trajectory is insensitive to all parameters regarding the load binding, i.e., parameters: k_{on}, k_{off}, k_8, k_9, k_{10}, k_{11}, k_{12} and the total promoter concentration p_T as it can be seen from Figure 2-7 (d). This is consistent with the fact that this system is insulated from the effects of the load. Thus, small variations in the binding affinity (k_{on}, k_{off}), promoter concentration (p_T) or complex phosphotransfer rates (k_8 through k_{12}) do not affect the X^{**} dynamics.

2.2.3 Output error sensitivity

Defining the output error as the squared difference between the X^{**} trajectories of the loaded and unloaded insulated system,

$$y(t,\lambda) = (X^{**}(t,\lambda) - X_L^{**}(t,\lambda))^2,$$

we can assess the sensitivity of the retroactivity attenuation property to parameters in λ, since we are directly comparing the behavior of the insulation device in isolation (system (2.26)-(2.32)with $p_T = 0$) and upon connection. This sensitivity is given by:

$$\frac{\partial}{\partial\lambda}y(t,\lambda) = 2(X^{**}(t,\lambda) - X_L^{**}(t,\lambda))\left(\frac{\partial}{\partial\lambda}X^{**}(t,\lambda) - \frac{\partial}{\partial\lambda}X_L^{**}(t,\lambda)\right). \qquad (2.54)$$

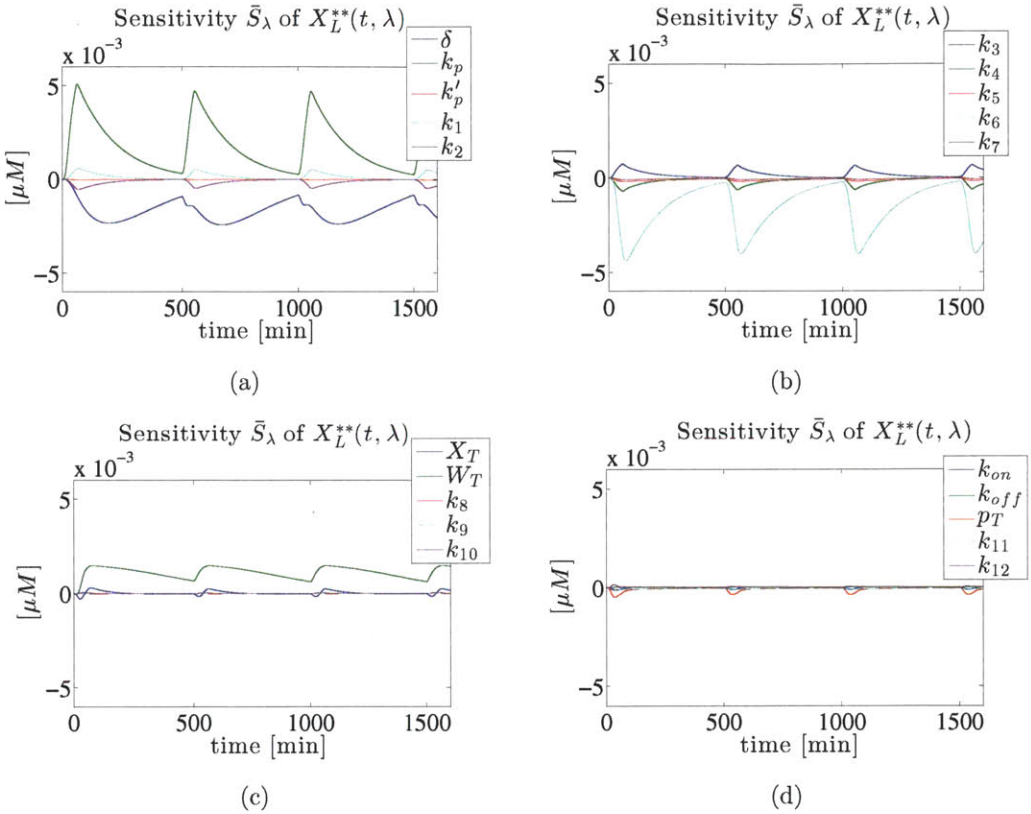

Figure 2-7: Dynamic sensitivity of the loaded insulated system. The dynamic sensitivity given by (2.53) was calculated across all insulated system parameters with nominal parameters given in Table B-2 final fit set. The simulations present the normalized dynamic sensitivity given by multiplying the solution of (2.53) by the diagonal matrix D_λ containing all parameter values. The loaded insulated system is most sensitive to parameters δ and k_p of the STAT5 reactions and the SKN7 dephosphorylation rate k_6 as the unloaded insulated system. Additionally it is more sensitive to the total SKN7 concentration X_T and the total YPD1 concentration W_T, as can be seen upon comparison with Figure 2-6. The system is insensitive to all parameters regarding the load: the association and dissociation rates k_{on} and k_{off}, the phosphotransfer rates k_8 through k_{12} and the total promoter site concentration p_T. This is consistent with the insulation device output dynamics being insulated from the effects of load.

Multiplying $\frac{\partial}{\partial\lambda}y(t,\lambda)$ on the right hand side by the diagonal parameter matrix $D_\lambda = \text{diag}\{\lambda_1, \lambda_2, \ldots, \lambda_n\}$ we can define the output error sensitivity as the change in the error between the trajectories of the insulated loaded and unloaded system due to a percentile change in the parameters λ. The simulation results for the normalized output error sensitivity are given in Figure 2-8.

Positive error sensitivity indicates an increase in the squared error, while a negative error sensitivity corresponds to a decrease. From Figure 2-8 (c), we see that the output error is most sensitive to the total phosphatase concentration W_T and to the dephosphorylation rate constant k_6. Increasing these parameters leads to an improvement in the insulation device performance. It was shown in Section 2.1.4 equation (2.51) that increasing either of these two parameters leads to a reduction in the effects of the retroactivity flux $\hat{s}_3$ thus isolating the dynamics from load, which translates to a decrease in the squared error. The output error is also sensitive to parameter k_p, which has positive sensitivity as seen in Figure 2-8 (a). It was discussed in Section 2.2.1 that increasing this parameter leads to an increase in the amplitude of Z^* which leads to a larger X^* and X^{**}. Having a high signal reduces the amount of available substrate X which can be phosphorylated and bind to the downstream load, as it can be seen from the conservation laws of model I1-I8. Increasing the concentration of X^* and X^{**} leads to an increased formation of C^* and C^{**}, which in turn affect the concentration of all insulation device species at the quasi-steady state. This effect is captured in the boxed terms of equation I3 and I4. Thus, an increase in k_p leads to a reduction of the substrate availability, which is detrimental to the load drivers performance.

2.2.4 Retroactivity attenuation performance

The property of the circuit was further assessed by simulating the mean squared error to the same T = 500 [min] square wave given by:

$$E = \frac{1}{T}\int_0^T \left[\frac{X^{**}(t) - X_L^{**}(t)}{\max[X^{**}(t)]}\right]^2 dt. \tag{2.55}$$

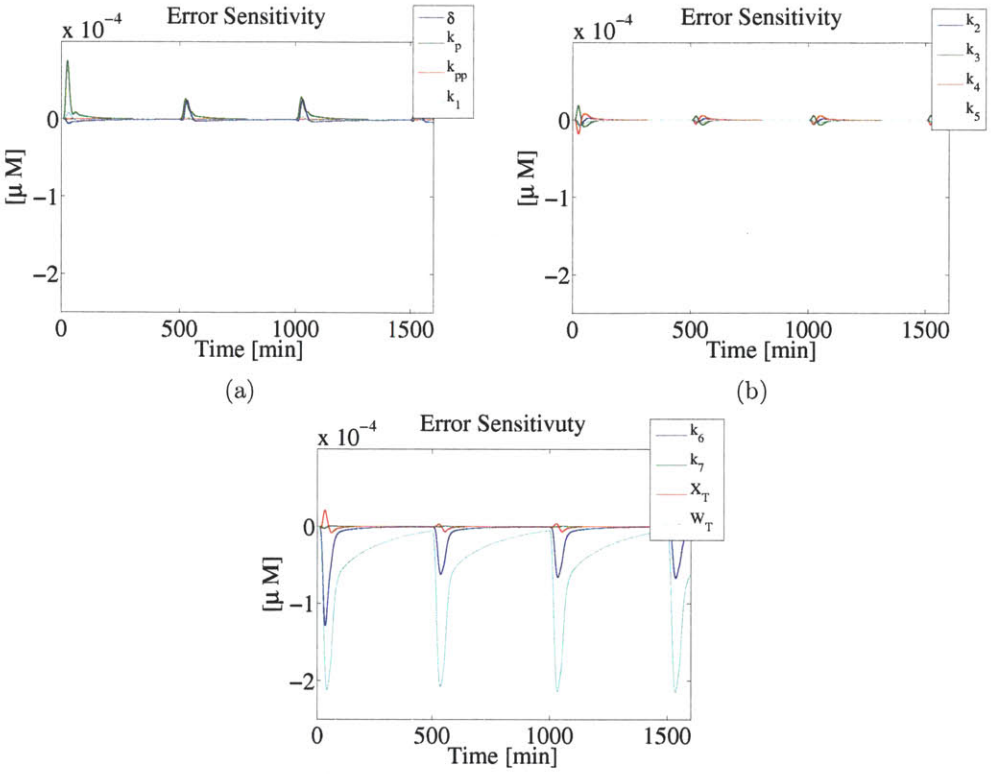

Figure 2-8: Error sensitivity of the insulation device. The error sensitivity given in (2.54) was calculated from the normalized dynamic sensitivities to the loaded and unloaded insulated systems as well as load drivers output trajectory from both. The analysis reveals that the output error performance is highly sensitive to the total YPD1 concentration W_T and the SKN7 dephoshorylation rate k_6. These two parameters where related to the retroactivity flux attenuation in (2.51), thus percentage increase in their values leads to a reduction in the system output error. This analysis demonstrates that the total phosphatase concentrations as well as spontaneous dephosphorylation rates of the insulation device are the key parameters of the retroactivity attenuation property.

The analysis was performed in two ways. First, the timescale of the insulation device reactions was increased in expressions (2.41)-(2.44) by increasing gain $G = 1/\epsilon$. The output error (2.55) was calculated, under different promoter sites concentrations, as gain G was increased. The simulations were performed keeping a fixed ratio X_T/p_T to prevent quasi-steady state effects. This illustrates the relevance of time scale separation in retroactivity attenuation. Second, the output error (2.55) was calculated as the total substrate and phosphatase concentration (X_T and W_T) were proportionally increased under different promoter sites concentrations. This is relevant since, from a design perspective, X_T and W_T constitute the tunable physical parameters in the system.

Retroctivity attenuation dependence on timescale

The insulation device dependence on timescale was evaluated by simulating the normalized system (2.40)-(2.46) once $G = 1/\epsilon$ in (2.41)-(2.44) was changed. Changing this gain in simulation corresponds to changing the timescale of the fast processes. The mean squared error in (2.55) was calculated across a range of $P_{TR-SSRE}$ promoter sites concentration, which is the physical quantity controlling the amount of load placed on the insulation device. To prevent from changes in the quasi-steady state of the system (2.40)-(2.46) when changing the load p_T, the total substrate concentration X_T was increased proportionally to p_T keeping the original p_T/X_T ratio fixed across all simulations.

From the simulation results shown in Figure 2-9 (a)-(d) we can see that the error increases, as the amount of promoter sites is increased for constant G. This behavior is expected since increased load concentration imparts higher retroactivity fluxes s_1, s_2 s_3 on the I1-I8 system dynamics. Conversely, the mean squared error decreases as the gain G is increased. This implies that the insulated system is able to attenuate higher retroactivity effects as the reactions encompassing the insulation device become faster. We can also see from Figure 2-9 (a)-(b) that the relationship between timescale increase and promoter sites increase is about linear for a fixed error level. Yet, for

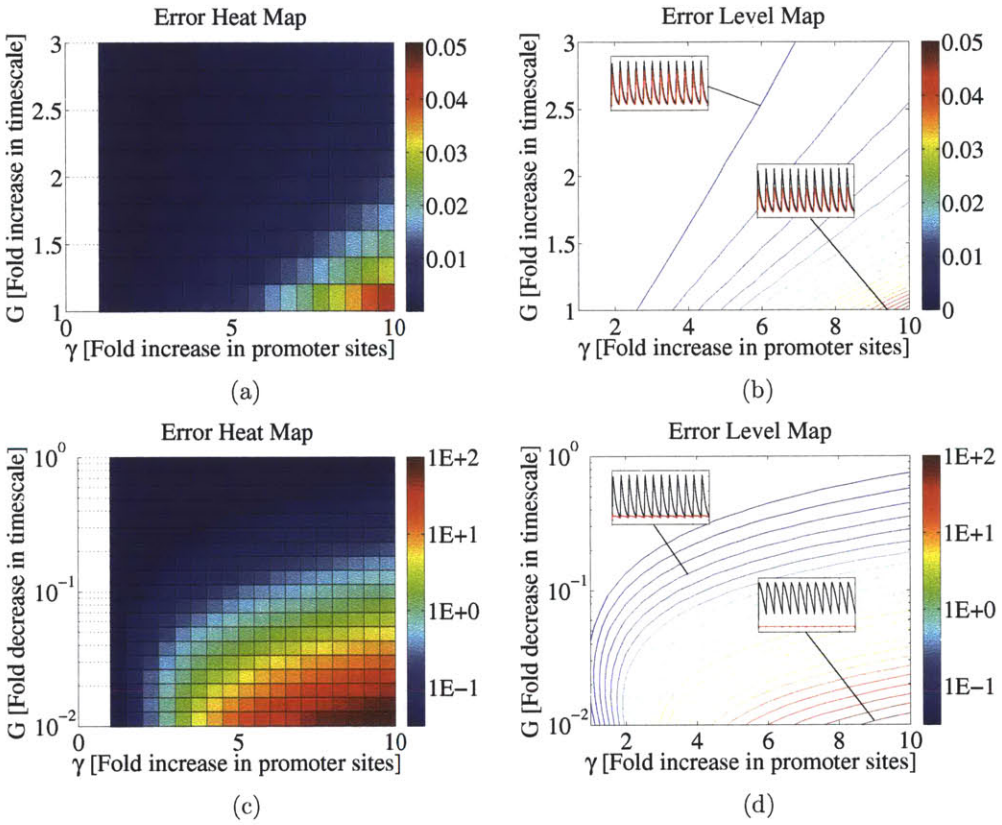

Figure 2-9: Mean squared output error heatmap for various insulation device phosphotransfer reaction timescales with increasing promoter sites. In this simulation the constant G represents the increase in timescale (a)-(b) or decrease of timescale (c)-(d) of the internal insulation device phosphotransfer reactions. It reports the error(2.55) for the simulated system (2.40)-(2.46) with varying promoter site concentrations $p_T = \gamma p_T^0$ where p_T^0 is the total promoter site concentration reported in Table B-1 final fit set. The simulation reveals that the fast internal dynamics of the insulation device indeed allows for retroactivity attenuation, behaving almost linear for a given error level at higher G, as can be seen from (b). When the insulation device reactions speeds are slowed down, to the extent of the slow processes in the insulated system, as shown in (c)-(d) the error is increased. This is consistent with the principle of timescale separation controlling the insulation device retroactivity attenuation property.

small error values, the required increase of G is larger. From Figure 2-9 (c)-(d) we see that the error increases as the timescale of the phosphotransfer reactions is reduced to the extent of the slower internal processes in the system. This demonstrates it is imperative to have a difference of timescales, meaning faster phosphotransfer reactions, for the insulation device to exhibit the retroactivity attenuation property.

Retroactivity attenuation dependence on the total substrate and phosphatase concentration

Assuming $\alpha = X_T/W_T$ is kept constant, system I1-I8 was simulated, by increasing proportionally both the substrate and phosphatase concentrations. The error due to an increase in $P_{TR-SSRE}$ promoter sites concentration was then calculated using expression (2.55). From the simulation results shown in Figure 2-10 (a)-(d) we can see that the error increases as the amount of promoter sites is increased, but decreases as the total substrate and phosphatase concentrations were increased for all values of the load. This is in accordance with the fact that these two factors are directly related to the retroactivity attenuation property of the insulation device as in equation (2.51).

Having high substrate prevents from quasi-steady states changes in system I1-I8 due to the load. Furthermore, in the case where the reactions with timescale k_1W_T, k_2W_T, k_3W_T, and k_4W_T are rate limiting (or slowest), increasing W_T improves the approximation $\epsilon \approx 0$, as it follows from the definition of ϵ given in Section 2.1.3. Thus, the dynamics of X^{**} can be approximated by the dynamics of the reduced system where the effects of the load are not present as seen in (2.47)-(2.50). Increasing W_T, thus leads to a preservation of the unloaded dynamics of the system when the phosphorylation reactions driven by YPD1 are rate limiting. Furthermore, decreasing both X_T and W_T concentrations have adverse effects on the load drivers performance as seen in Figure 2-10 (c)-(d). Meaning the retroactivity attenuation property requires a minimal concentration of substrate and phosphatase for its successful implementation.

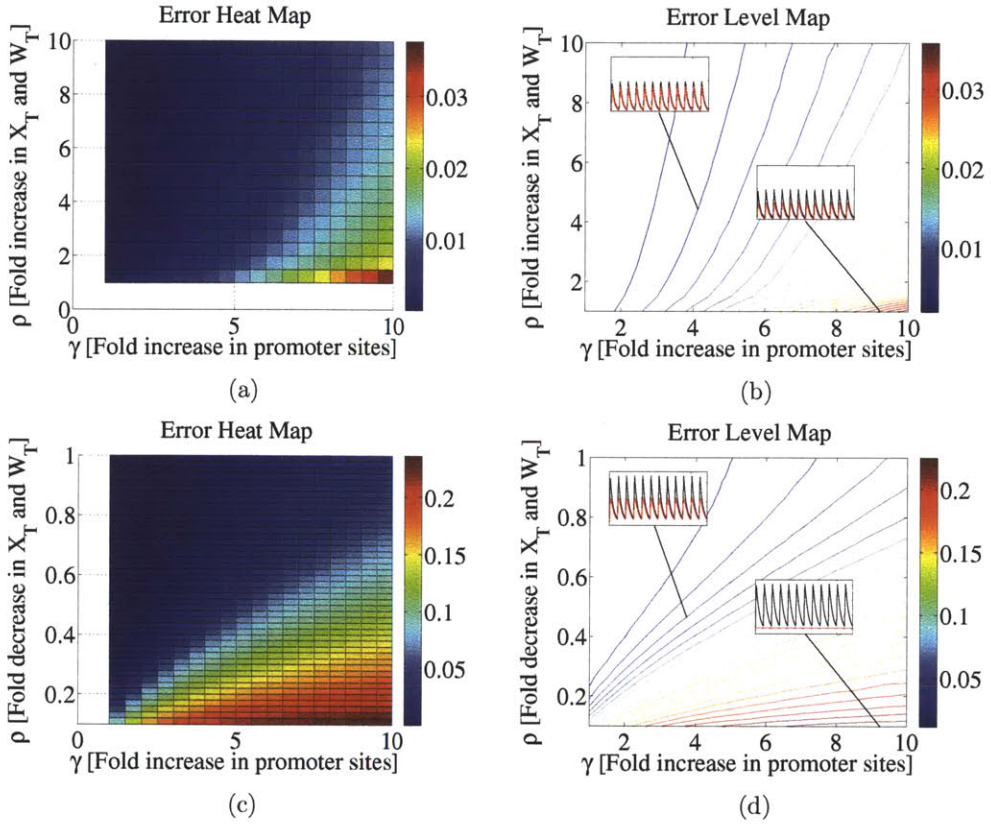

Figure 2-10: Mean squared output error heatmap for various insulation device total substrate and phosphatase concentrations with increasing promoter sites. In these simulations ρ provides the fold increase or decrease in the total SKN7 concentration X_T and YPD1 concentraition W_T. The reported error was calculated applying (2.55) for the simulated system I1-I8, with promoter sites concentrations given by $p_T = \gamma p_T^0$ where p_T^0 is the total promoter site concentration reported in Table B-1 final fit set. The simulation demonstrates that high substrate and phosphatase concentrations allows for retroactivity attenuation as seen in (a)-(b). This is consistent with (2.51), where X_T and W_T are directly related to the attenuation of the retroactivity flux in the load drivers output dynamics. On the other hand, a decrease in these concentrations leads to a higher error as see in (c)-(d). Thus, the total substrate and phosphatase concentrations are good tunable parameters to improve the retroactivity attenuation property of the insulation device.

2.2.5 Steady state sensitivity

Another interesting feature of this experiment is that both the insulated and uninsulated system have the same steady state response to different DOX induction levels. A way to understand what parameters have a larger weight on this steady state characteristic is to perform a steady state error sensitivity analysis on the GFP output concentration of both insulated and uninsulated circuits for all values of DOX. Recalling G_m as the GFP concentration of the uninsulated system and G as the GFP concentration of the insulated system, we can define the squared GFP error as:

$$H(DOX, \lambda) = (G_m(DOX, \lambda) - G(DOX, \lambda))^2, \tag{2.56}$$

where the $G_m(DOX, \lambda)$ is the steady state value of G_m in system U1-U3 and the $G(DOX, \lambda)$ is the steady state value of G in system I1-I8 at different DOX concentrations.

The steady state sensitivity of $X(t, \lambda)$ can be obtained by setting $\dot{S}_\lambda = 0$ in (2.53) and solving for S_λ which gives:

$$S_\lambda = -\left(\frac{\partial f(t, X, \lambda)}{\partial X}\right)^{-1} \frac{\partial f(t, X, \lambda)}{\partial \lambda}. \tag{2.57}$$

We can measure the sensitivity of the steady state error to all parameters in both insulated and uninsulated unloaded systems by defining the parameter vector $\lambda = (\delta,$ $k_p,$ $k_p,$ $k_1,$ $k_2,$ $k_3,$ $k_4,$ $k_5,$ $k_6,$ $k_7,$ $X_T,$ $W_T,$ $k_m,$ $K_{dox},$ $k_g,$ $K_{gfp},$ $\delta_G,$ $\delta_X)^T$ and taking the partial derivative with respect to λ of (2.56):

$$\frac{\partial}{\partial \lambda} H(DOX, \lambda) = 2(G_m(DOX, \lambda) - G(DOX, \lambda))(\bar{S}_\lambda^{G_m} - \bar{S}_\lambda^{G}). \tag{2.58}$$

Expressions $\bar{S}_\lambda^{G_m}$ and $\bar{S}_\lambda^{G}$ are the normalized steady state sensitivity of GFP to parameters in λ at a given DOX level. They are obtained by calculating (2.57) then multiplying on the right hand side by $D_\lambda = \text{diag}\{\lambda\}$, i.e., $\bar{S}_\lambda^{G_m} = S_\lambda^{G_m} D_\lambda$.

The steady state error sensitivities are given in Figure 2-11. These plots were generated using expression (2.58), where the GFP concentration was simulated for

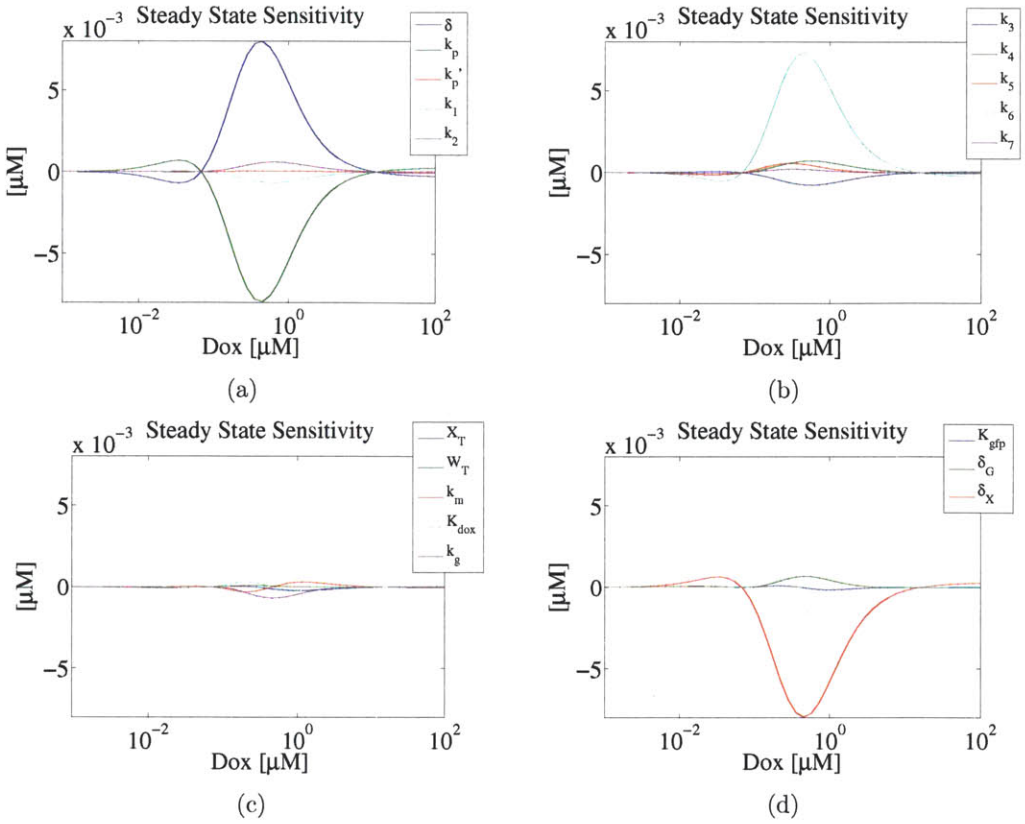

Figure 2-11: Steady state error characteristic sensitivity. The steady state sensitivity given in (2.58) was calculated for all insulated and uninsulated system parameters, with nominal values given in Table B-1 & Table B-2 final fit set. The simulations reveal that the steady state characteristic of both systems is mostly insensitive to parameters shared between systems, specifically k_m, K_{dox}, k_g, K_{gfp}, and δ_G. Furthermore, it shows higher sensitivity to insulated system parameters δ, k_p and k_6, consistent with the unloaded insulated system dynamic sensitivity; and to parameter δ_X of the uninsulated system. The analysis reveals that the biggest steady state effects are given by parameters that have the biggest impact on the output of both the uninsulated and insulated systems independently.

insulated and uninsulated systems and their sensitivity calculated for a range of DOX values. As for the output error sensitivity presented in Section 2.2.3, positive sensitivity implies an increase in error between the G and G_m steady state characteristic. Similarly, negative error sensitivity implies a reduction in the steady state characteristic error. The general result is that only parameters that might affect the X^{**} amplitude in the insulated system or the X_m amplitude in the uninsulated system independently, have a significant effect on the steady state output error. We can further claim that all parameters shared between the two systems, meaning the coefficients for the Hill function of the P_{TET} and $P_{TR-SSRE}$ promoters as well as the GFP degradation, have no significant effect on the steady state output error, relative to the parameters not shared between the two systems as seen in Figure 2-11 (a)-(d). Specifically, the parameters shared between the two systems are: k_m, K_{dox}, k_g, K_{gfp}, and δ_G. As discussed in Section 2.2.1, the dynamics of X^{**} which are reported by G, are sensitive to decay parameter δ and phosphorylation rate k_p, which accounts for the high steady state sensitivity as seen in Figure 2-6 (a) and Figure 2-7 (a). This is due to the fact that both of these parameters affect directly the amplitude of Z^* which is the input to the insulation device, as discussed in Section 2.2.1. Thus, small variations on these is reflected on the concentration X^{**} and ultimately in G. Based on Figure 2-11 (a), increasing δ increases the steady state characteristic error while increasing k_p decreases it. It was also discussed in Section 2.2.1 that the X^{**} trajectory is highly sensitive to the desphosphorylation rate k_6 as seen in Figure 2-6 (c) and Figure 2-7 (b). Increasing this parameter leads to a higher dephosphorylation of X**, thus decreasing its concentration which results in decreasing G. From Figure 2-11 (b), increasing this parameter leads to an increase in the error between G and G_m. Conversely, increasing the degradation rate δ_X decreases the amplitude of X_m, which leads to a decrease in G_m, and from Figure 2-11 (d), decreases the steady state error as well. Thus, parameters that provide the greatest sensitivity to the amplitude of X^{**} independent from the amplitude of X_m, and vice versa, have the greatest impact on the steady state error.

To further explore how the parameters to which the steady state error is more

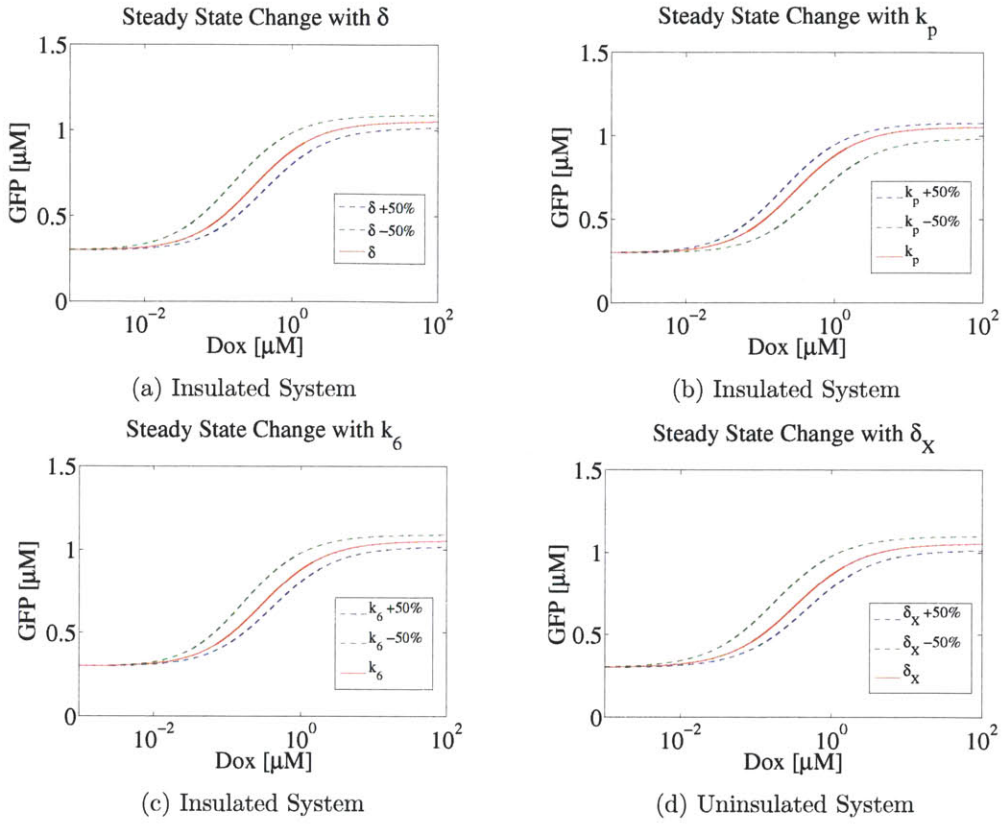

(a) Insulated System

(b) Insulated System

(c) Insulated System

(d) Uninsulated System

Figure 2-12: Steady state characteristic dependence on parameters. The steady state characteristic of both insulated and uninsulated systems was simulated for 50% increase and decrease in the parameters that prov ided the highest sensitivity in Figure 2-11. The panels (a)-(c) show an envelope of the insulated system steady state characteristic, while panel (d) shows an envelope for the uninsulated system steady state characteristic. Variations in these parameters, which are not shared between systems, leads to deviations in the steady state characteristic of the insulated and uninsulated system from being almost the same.

sensitive to affect the steady state characteristic, plots for 50% variations in parameters $\{\delta,\ k_p,\ k_6,\ \delta_X\}$ were generated to bound the maximum and minimum change given by each of them as seen in Figure 2-12. From Figure 2-12 (a) and Figure 2-12 (c), we can see that parameter δ modeling de decay of Z and Z^* as well as parameter k_6 modeling the dephosphorylation of X^{**}, of the insulated system, have a similar qualitative effect on the steady state. Both of them decrease the overall steady state characteristic for a 50% increase in their value, while increasing the steady state curve for a 50% decrease in their value. This is expected since δ models the decay of Z^*, the insulation device input as seen in Section 2.2.1. Increasing this decay decreases the input, thus X^{**} which is reported by G. Similarly k_6 decreases X^{**}, thus lowering the G across all DOX values. Conversely, from Figure 2-12 (b) we can see that increasing k_p by 50%, which models the phosphorylation of Z into Z*, increases the concentration of GFP across all DOX values. Increasing this parameter results in an increase in Z^*, which translates to higher X^{**} and thus the concentration of GFP. Decreasing this parameter by 50%, decreases the overall steady state characteristic. Finally, from Figure 2-12 (d) we can see that increasing δ_X modeling the decay of X_m, of the uninsulated system, reduces the steady state characteristic across all DOX values. A 50% increase in this value leads to a decrease in the X_m concentration, thus reducing the GFP concentration. A 50% decrease has the opposite effect, so it increases the GFP concentration across all DOX values.

2.3 Discussion

From this analysis we see that the insulation device allows the insulated system preserve its isolated dynamic performance in the presence of the load. The operational principle relies on timescale separation, where the insulation device output protein SKN7 successfully tracks the slow transcriptional signal of the input device since its dynamics evolve in a faster timescale. Specifically, due to the slow input signal SKN7 is able to quickly reach its quasi-steady state even in the presence of load. Furthermore, since the SKN7 is in high abundance the quasi-steady state is unaffected

by the load, thus isolating from both dynamic and steady state effects. The reason why the quasi-steady state of SKN7 remains unaffected was appreciated through a flux analysis. As it was depicted in Figure 2-2 when the phosphorylation and dephosphorylation fluxes of SKN7, dependent on the phosphotransfer kinetic rates and total concentration of YPD1, are high enough the effect of the additional flux due to load is attenuated. This makes the SKN7 output dynamics independent of the load, therefore attenuating retroactivity effects. This result provides then that the key parameters for the retroactivity attenuation property are the total phosphatase concentration and the phosphotransfer kinetic rates. And indeed from the sensitivity analysis we saw that the insulation device output error is highly sensitive to the total YPD1 concentration (W_T) and the desphosphorylation rate k_6.

It was also shown by simulation in Figure 2-9 that the insulation device error could be mitigated for higher load by increasing phosphotransfer reactions timescale of the insulation device. The inherently fast timescale due to the nature of the phosphotransfer reaction, allows that for a given error the relationship between increase in promoter sites and insulation device timescale is almost linear. Furthermore, reducing the phosphorylation timescale scaled nonlinearly with the insulation device output error, thus being detrimental to the device performance. Since the timescale of the YPD1 mediated phosphotransfer reactions can be tuned by increasing the total YPD1 concentration, the simulations presented in Figure 2-10 further demonstrate the validity of using the total YPD1 and SKN7 concentrations as the easy tunable parameters in the system to further reduce the output error.

Furthermore, it was shown experimentally (data pending publication), that the steady state characteristic was preserved in the presence of load for both insulated and uninsulated systems. For the uninsulated system this is consistent with the SNK7m-$P_{TR-SSRE}$ complex being protected from degradation. As we can see from the system equations U1-U3 the steady state of SKN7m is not dependent on the load. This can be accounted for physically by the constant production of SKN7m generating enough protein to allow the bound SKN7m reach its steady state value while maintaining the free steady state concentration is unaffected. The insulated system is able to preserve

its steady state characteristic given SKN7 is insufficiently high amount relative to the $P_{TR-SSRE}$ concentration. Moreover, the steady state characteristic is preserved between both insulated and uninsulated system for a specific range of parameters of the insulation device.

Chapter 3

Tradeoffs in the design of insulation devices

In this chapter, a single phosphorylation cycle model is proposed for the further analysis of the phosphorylation based insulation device. The insulation device output is parameterized with the cycle substrate and phosphatase concentrations to determine an optimal amount that minimizes the retroactivity to the input and retroactivity to the output. The approach to characterize this tradeoff is based on singular perturbation and contraction theory. An upper bound is determined on the steady state error between the output of the insulation device under study and an ideal insulation device. This upper bound is a function of the substrate and phosphatase concentrations and can be minimized with respect to these variables. It is then shown through simulation that the calculated upper bound is tight.

3.1 Mathematical tools

Theorem 1. *(Contraction Theorem):* Adapted from [24]. Consider the n-dimensional deterministic system $\dot{x} = f(x,t)$, where f is a smooth nonlinear function. The system is said to be contracting if any two trajectories, starting from different initial conditions, converge exponentially to each other. A sufficient condition is the existence of some matrix measure, m, such that there is a $\lambda > 0$ with $m\left(\frac{\partial f(x,t)}{\partial x}\right) \leq -\lambda$ for all x

and for all $t \geq 0$. The scalar λ defines the contraction rate of the system.

Throughout this paper, the vector norm $|\cdot|$ will refer to the ℓ^2-norm given by $|x|_2 = \left(\Sigma_{j=1}^n |x_j|^2\right)^{1/2}$ and $m_2(A)$ the induced matrix measure given by $m_2(A) = \max_i \left(\lambda_i \left\{\frac{A+A^*}{2}\right\}\right)$ where λ_i denotes the matrix's i^{th} eigenvalue.

Lemma 1. *(Robustness):* Adapted from [24]. Assume that the system

$$\dot{x} = f(x,t) \tag{3.1}$$

is contracting, with contraction rate λ, and consider the perturbed system

$$\dot{x}_p = f(x_p,t) + d(x_p,t), \tag{3.2}$$

where $d(x_p,t)$ is bounded, so there is a $\bar{d} \geq 0$ such that $|d(x_p,t)| \leq \bar{d}$ for all x_p and for all $t \geq 0$. Then, the trajectory of the perturbed system satisfies

$$|x_p(t) - x(t)| \leq e^{-\lambda t}|x_p(0) - x(0)| + \frac{\bar{d}}{\lambda}. \tag{3.3}$$

Lemma 2. Adapted from [25]. Assume that the system $\dot{x} = f(x,z(t))$ is partially contracting in x with contraction rate λ_x so that the solution of the system $f(x_s,z(t)) = 0$ can be written as $x_s = \gamma(z)$, i.e., there is a unique global mapping between x and z. Assume further that there exists a $\bar{d} \geq 0$ such that $\left|\frac{\partial \gamma(z)}{\partial z}\dot{z}\right| \leq \bar{d}$ for all x, for all z and for all $t \geq 0$. Then, any trajectory $x(t)$ satisfies

$$|x(t) - \gamma(z(t))| \leq e^{-\lambda_x t}|x(0) - \gamma(z(0))| + \frac{\bar{d}}{\lambda_x}. \tag{3.4}$$

Proof. Let x be the solution of $\dot{x} = f(x,z(t))$ while $x_s = \gamma(z(t))$ is the solution of the "perturbed" system $\dot{x}_s = f(x_s,z(t)) + \frac{\partial \gamma(z)}{\partial z}\dot{z}$ with disturbance $\frac{\partial \gamma(z)}{\partial z}\dot{z}$. Applying the result (3.3) from Lemma 1 yields bound (3.4). □

Proposition 1. Consider the system (3.1)-(3.2) in Lemma 1 and let $|d(x_p,t)| \leq C_0 + \sum_{k=1}^n C_k\, e^{-\lambda_k t}$. Having $x_0 = |x(0) - x_p(0)|$, the upper bound on $|x(t) - x_p(t)|$ is

given by

$$|x(t) - x_p(t)| \leq x_0 e^{-\lambda t} + \frac{C_0}{\lambda} + \sum_{k=1}^{n} \frac{C_k}{\lambda - \lambda_k} e^{-\lambda_k t}. \tag{3.5}$$

Proof. Let $X(t) = |(x_p(t) - x(t))|$, then $\frac{dX}{dt} + \lambda X \leq |d(x_p, t)| \leq C_0 + \sum_{k=1}^{n} C_k\, e^{-\lambda_k t}$ as in [24]. Multiplying by the integrating factor $e^{\lambda t}$ we can re-write the differential equation as $\frac{d}{dt}(e^{\lambda t} X) \leq e^{\lambda t}\left(C_0 + \sum_{k=1}^{n} C_k\, e^{-\lambda_k t}\right)$. The differential equation can now be integrated to obtain (3.5) where the terms with negative coefficients were neglected for the approximation. □

3.2 System model and problem description

A phosphorylation cycle consists of a set of two reversible enzymatic reactions, where the activation and deactivation of a substrate through the addition/removal of a phosphate group is used to transmit information to a downstream system [26]. Throughout this work, for a given species X its concentration is denoted by X (italics). In a phosphorylation cycle, a kinase labeled Z, regulated by $k(t)$, activates substrate X through a phosphate transfer reaction to form X*, while Y deactivates X* to form X. Protein X* also regulates a downstream system by binding to sites p forming complex C. These sites can be DNA promoter sites if X* is a transcription factor or they can belong to a substrate if X* is an active kinase. The chemical reactions for the system are:

$$\begin{aligned}
&\phi \xrightarrow{\mathrm{k(t)}} \mathrm{Z}\,, \\
&\mathrm{Z} \xrightarrow{\delta} \phi, \\
&\mathrm{X} + \mathrm{Z} \underset{\beta_2}{\overset{\beta_1}{\rightleftharpoons}} \mathrm{C_1} \xrightarrow{k_1} \mathrm{X^*} + \mathrm{Z}\,, \\
&\mathrm{X^*} + \mathrm{Y} \underset{\alpha_2}{\overset{\alpha_1}{\rightleftharpoons}} \mathrm{C_2} \xrightarrow{k_2} \mathrm{X} + \mathrm{Y} \\
&\mathrm{X^*} + \mathrm{p} \underset{k_{off}}{\overset{k_{on}}{\rightleftharpoons}} \mathrm{C},
\end{aligned}$$

in which C_1 is the complex formed by the substrate X and kinase Z and C_2 is the complex formed by the protein X^* and phosphatase Y. The assumed conservation laws are: $X_T = X + X^* + C_1 + C_2 + C$, $Y_T = Y + C_2$, and $p_T = p + C$.

The ODE model of the phosphorylation cycle is given by:

$$\begin{aligned}
\frac{dZ}{dt} &= k(t) - \delta Z \overbrace{-\beta_1 Z X_T \left(1 - \frac{X^*}{X_T} - \frac{C_1}{X_T} - \frac{C_2}{X_T} - \frac{C}{X_T}\right) + (\beta_2 + k_1) C_1}^{r}, \\
\frac{dC_1}{dt} &= \beta_1 Z X_T \left(1 - \frac{X^*}{X_T} - \frac{C_1}{X_T} - \frac{C_2}{X_T} - \frac{C}{X_T}\right) - (\beta_2 + k_1) C_1, \\
\frac{dC_2}{dt} &= -(k_2 + \alpha_2) C_2 + \alpha_1 Y_T X^* \left(1 - \frac{C_2}{Y_T}\right), \\
\frac{dX^*}{dt} &= k_1 C_1 + \alpha_2 C_2 - \alpha_1 Y_T X^* \left(1 - \frac{C_2}{Y_T}\right) \overbrace{+ k_{off} C - k_{on} X^* (p_T - C)}^{s}, \\
\frac{dC}{dt} &= -k_{off} C + k_{on} X^* (p_T - C).
\end{aligned} \tag{3.6}$$

Here, r represents the retroactivity to the input and s represents the retroactivity to the output. One can abstract the signal flow in (3.6) using system Σ in Figure 3-1. Signal Z drives the X^* dynamics through complex C_1 while the binding and unbinding reaction of Z with X creates retroactivity r in the Z dynamics. Similarly, X^* drives the C dynamics downstream, while being affected by the retroactivity s. An ideal insulation device should behave as system Σ_I in Figure 3-1 where the terms under brace r and s in (3.6) were set to zero.

The key tunable parameters in this system are X_T and Y_T, which will be kept at a constant ratio $Y_T/X_T = \rho$ throughout the analysis. We seek to adjust the values of these parameters in such a way that the behavior of the system is close to that of an ideal insulation device. This can be better appreciated in Figure 3-2, where different substrate concentrations are tested using a sinusoidal input $k(t)$ on system (3.6). The black line describes the ideal behavior X_I^* given by $r, s = 0$. The red line is the behavior of X^* in the system having $r, s \neq 0$. As we can see from Figure 3-2, having too high or too low values of X_T leads to an error between the actual X^* and the ideal X_I^* device responses. The reason being that a large X_T

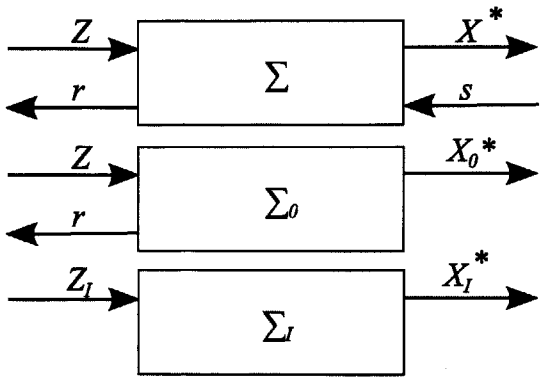

Figure 3-1: Insulation device virtual subsystems. Top: system Σ with input Z, output X^*, retroactivity to the input r and retroactivity to the output s. Middle: System Σ_0 with input signal Z subject to retroactivity r, while output signal X_0^* has retroactivity to the output $s = 0$. Bottom: system Σ_I is the ideal realization of system Σ, where both signals Z_I and X_I^* are not subject to retroactivity.

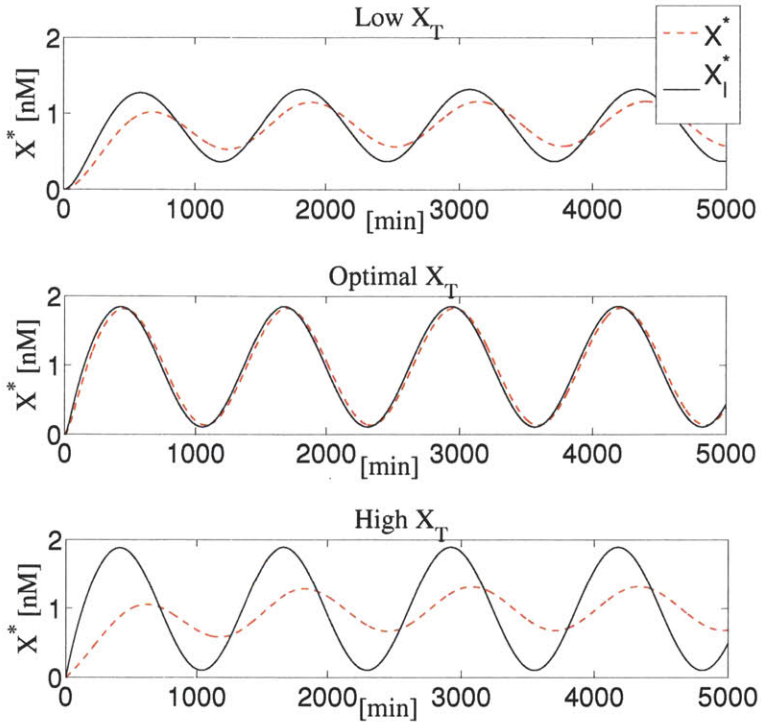

Figure 3-2: Effect of substrate concentration on the insulation device output. The red line is output X^* of system Σ in Figure 3-1 and the black line is output X_I^* of system Σ_I, with different substrate concentrations. In all simulations, the parameters are taken from [27]: $k_{off} = 10$ min^{-1}, $k_{on} = 1$ (nM min)$^{-1}$, $\delta = 0.01$ min^{-1}, $k(t) = \delta(1 + sin(\omega t))$, and $\omega = 0.005$ min^{-1}. Also $k_1 = k_2 = 0.6$ min^{-1}, $\alpha_1 = \beta_1 = .006$ (nM min)$^{-1}$, $\beta_2 = \alpha_2 = 6$ min^{-1}, $p_T = 10$ nM and $\rho = 1$. Low $X_T = 10$ nM, intermediate $X_T = 100$ nM and high $X_T = 1000$ nM.

concentration applies a load to the $Z(t)$ dynamics changing the nominal signal $Z_I(t)$, while attenuating the effect of p_T on the $X^*(t)$ dynamics. This tradeoff between minimizing the effect of r and s is studied in this paper. Specifically, the total output error $\Delta X^*_{TOT}(t) := X^*(t) - X^*_I(t)$, is quantified by determining positive functions, $A(X_T)$, $B(X_T)$, $\lambda(X_T)$ such that$|\Delta X^*_{TOT}| \leq A(X_T)e^{-\lambda(X_T)t} + B(X_T)$.

3.3 Solution approach

This problem will be solved by quantifying the errors in X^* due to r and s in (3.6) to find $A(X_T)$, $B(X_T)$ and $\lambda(X_T)$. To this end, the virtual system Σ_0 in Figure 3-1 is obtained from Σ by setting $s = 0$. The output error is defined as $\Delta X^*_0(t) := X^*(t) - X^*_0(t)$, which accounts for the error in $X^*(t)$ only due to retroactivity s. Likewise, the virtual system Σ_I in Figure 3-1 is obtained from Σ by setting $r = 0$ and $s = 0$. The input error, defined as $\Delta X^*_I(t) := X^*_0(t) - X^*_I(t)$, accounts for the error in $X^*_0(t)$ due only to retroactivity to the input r. It will be shown that the total output error, given by $\Delta X^*_{TOT} = X^*(t) - X^*_I(t)$, can be upper bounded by $|\Delta X^*_{TOT}(t)| \leq |\Delta X^*_0(t)| + |\Delta X^*_I(t)|$. We proceed to separately determine the output error and input error.

First, a system order reduction will be performed through singular perturbation to obtain a two-state variable model for $Z(t)$ and $X^*(t)$. Processes in system (3.6) occur in three timescales [8]. The slowest timescale is that of the kinase dynamics due to protein production and decay and the intermediate timescale is that of phosphorylation. The fastest timescale is that of the binding and unbinding reactions to form complexes C_1, C_2 and C. Thus, singular perturbation parameters $\epsilon_1 := \delta/k_1$ and $\epsilon_2 := \delta/k_{off}$ are selected so that $\epsilon_2 \ll \epsilon_1 \ll 1$. We define the parameters: $k_d := k_{off}/k_{on}$, $b_1 := \beta_1\epsilon_2/\delta$, $a_1 := \alpha_1\epsilon_2/\delta$, $b_2 := \beta_2\epsilon_2/\delta$, $a_2 := \alpha_2\epsilon_2/\delta$, and $k_x := k_2/k_1$. The transformation $w := Z + C_1$ and $y := X^* + C_2 + C$ is also performed on system (3.6), converting it to standard singular perturbation form [9]:

$$\frac{dw}{dt} = k(t) - \delta(w - C_1)$$

$$
\begin{aligned}
\epsilon_1 \frac{dy}{dt} =& \delta C_1 - k_x \delta C_2 \\
\epsilon_2 \frac{dC_1}{dt} =& \delta b_1 (w - C_1)(X_T - y - C_1) - \delta(b_2 + \epsilon_2/\epsilon_1) C_1 \\
\epsilon_2 \frac{dC_2}{dt} =& \delta a_1 (Y_T - C_2)(y - C_2 - C) - \delta(a_2 + k_x \epsilon_2/\epsilon_1) C_2 \\
\epsilon_2 \frac{dC}{dt} =& \frac{\delta}{k_d}(y - C_2 - C)(p_T - C) - \delta C.
\end{aligned} \tag{3.7}
$$

We let $Z(t, \epsilon_1, \epsilon_2)$ and $X^*(t, \epsilon_1, \epsilon_2)$ denote the Z and X^* trajectories of system (3.7) when transformed back to the original coordinates. This system is the same as described in Example 1 of [8]. Since it satisfies all the required conditions, one can use Lemma 2 (Case 1) of [8], which performs a nested application of Tikhonov's singular perturbation Theorem, to determine the reduced order dynamics.

3.3.1 Input error

To determine the input error $\Delta X_I^* = X_0^*(t) - X_I^*(t)$, the effect of r in the reduced order dynamics of $Z(t)$ will be analyzed. The error produced by r will be written as $\Delta Z(t) := Z(t) - Z_I(t)$, which acts as a disturbance in the dynamics of $X_0^*(t)$ leading to the error $\Delta X_I^*(t)$.

The kinase dynamics evolve in the slowest timescale, thus singular perturbation is performed by setting $\epsilon_1 = 0$ and $\epsilon_2 = 0$. Defining the phosphorylation and dephosphorylation dissociation constants as $k_{d1} = \beta_2/\beta_1$ and $k_{d2} = \alpha_2/\alpha_1$, respectively, and assuming $X^* \ll k_{d2}$, k_d, and $p_T \ll X_T$ (thus working in the linear regime of the Michaelis-Menten functions), the slow manifold is given by $\tilde{X}^* = \psi_x(\tilde{Z}) := \frac{\tilde{Z} X_T k_{d2}}{\tilde{Z}[k_{d2} + (k_x+1)Y_T] + k_x k_{d1} Y_T}$, $C_2 = \psi_2(\psi_x(\tilde{Z})) := \frac{Y_T}{k_{d2}} \psi_x(\tilde{Z})$, $C_1 = \psi_1(\psi_x(\tilde{Z})) := k_x \frac{Y_T}{k_{d2}} \psi_x(\tilde{Z})$, $C = \psi_c(\psi_x(\tilde{Z})) := \frac{p_T}{k_d} \psi_x(\tilde{Z})$. Variables $\tilde{X}$ and $\tilde{Z}$ denote the approximation of X and Z in system (3.7) once $\epsilon_1 = 0$ and $\epsilon_2 = 0$. The reduced order dynamics of $\tilde{Z}$ are obtained by differentiating the slow variable w with respect to time. We have that

$$
\frac{dw}{dt} = \frac{d\tilde{Z}}{dt} + \frac{dC_1}{dt} = \frac{d\tilde{Z}}{dt} + \frac{d\psi_1}{d\psi_x} \frac{d\psi_x}{d\tilde{Z}} \frac{d\tilde{Z}}{dt},
$$

so that

$$\frac{d\tilde{Z}}{dt} = \frac{1}{1 + \frac{d\psi_1}{d\psi_x}\frac{d\psi_x}{d\tilde{Z}}} \frac{dw}{dt},$$

which, employing the first equation in (3.7), can be expanded as

$$\frac{d\tilde{Z}}{dt} = (1 - R_z(\tilde{Z}))f_z(\tilde{Z}, k(t)), \tag{3.8}$$

where

$$\begin{aligned} R_z(\tilde{Z}) &:= \frac{k_{d1}X_T}{\left\{\tilde{Z}\left[\frac{k_{d2}}{Y_T k_x} + \frac{(k_x+1)}{kx}\right] + k_{d1}\right\}^2 + k_{d1}X_T}, \\ f_z(\tilde{Z}, k(t)) &:= k(t) - \delta\tilde{Z}. \end{aligned} \tag{3.9}$$

By proof of Case(1) in Lemma 2 of [8], one has that $\left|\tilde{Z}(t) - Z(t, \epsilon_1, \epsilon_2)\right| = O(\epsilon_1) + O(\epsilon_2/\epsilon_1)$, so for $\epsilon_1,\ \epsilon_2 \to 0$, $\tilde{Z}(t)$ will be taken as a good approximation of $Z(t, \epsilon_1, \epsilon_2)$, and be denoted by $Z(t)$ with abuse of notation.

Bound for $\Delta Z(t)$

From (3.8), it is notable that the reduced input dynamics have the form of a nominal contracting system with an additive disturbance. The nominal or isolated system is given by setting $R_z = 0$ in (3.8), that is,

$$\frac{dZ_I}{dt} = f_z(Z_I, k(t)). \tag{3.10}$$

The connected or perturbed Z dynamics are given by

$$\frac{dZ}{dt} = f_z(Z, k(t)) + h_z(Z, k(t)), \tag{3.11}$$

where the expression $h_z(Z, k(t))$ has been defined as

$$h_z(Z, k(t)) := -R_z(Z)f_z(Z, k(t)). \tag{3.12}$$

In order to apply the robustness result given in Lemma 1 to find a bound on ΔZ, we first need a bound on the perturbation $h_z(Z, k(t))$.

Claim 1. Define $\bar{k} := \max_{t\geq 0}|k(t)|$ and assume that $Y_T > \max\left\{\frac{2\bar{k}k_{d2}/k_x}{\delta k_{d1}/2-\frac{2\bar{k}(k_x+1)}{k_x}}, \frac{\bar{k}k_{d2}/\delta}{k_x k_{d1}-\bar{k}(k_x+1)/\delta}\right\}$ and $k_{d1} > \max\left\{\frac{4\bar{k}(k_x+1)}{\delta k_x}, \frac{\bar{k}}{\delta}\frac{(k_x+1)}{k_x}\right\}$.

Also let $z = \gamma_z(k)$ denote the globally unique solution of $f_z(z,k) = 0$ and define $V_z := \max_{t\geq 0}|\dot{k}(t)|$. Then, the upper bound on $h_z(Z, k(t))$ is given by

$$|h_z(Z, k(t))| \leq C_0^z e^{-G_z t} + C_1^z, \tag{3.13}$$

where $C_0^z := \delta\left(\frac{X_T}{X_T+k_{d1}}\right)\gamma_z^0$ and $C_1^z := \left(\frac{X_T}{X_T+k_{d1}}\right)\frac{V_z}{G_z}$, defining $\gamma_z^0 := |Z(0) - \gamma_z(Z(0))|$ and $G_z := \frac{\delta k_{d1}X_T/2+\delta k_{d1}^2}{(k_{d1}+X_T)^2}$.

Proof. See Appendix A-1. □

Claim 2. Let $\lambda_z = \delta$ be the contraction rate of system (3.10) and $\Delta Z_0 := |Z(0) - Z_I(0)|$, then we have

$$|\Delta Z(t)| \leq \Delta Z_0 e^{-\lambda_z t} + \frac{C_0^z}{\lambda_z - G_z}e^{-G_z t} + \frac{C_1^z}{\lambda_z}. \tag{3.14}$$

Proof. In order to apply Lemma 1 to system (3.10) - (3.11), the contraction rate λ_z of the isolated system (3.10) is obtained. This is a positive number such that $m_2\left(\frac{\partial f_z(Z_I,k(t))}{\partial Z_I}\right) \leq -\lambda_z$, and it is given by $\lambda_z = \delta$. From Claim 1, since (3.13) satisfies Proposition 1, we have (3.14). □

The assumptions on Claim 1 are satisfied for Y_T and k_{d1} sufficiently large. Also, after a transient, the input error is bounded by

$$\lim_{t\to+\infty}|\Delta Z(t)| \leq \frac{C_1^z}{\lambda_z} = \frac{X_T(k_{d1}+X_T)\frac{V_z}{\delta}}{\delta k_{d1}(\frac{X_T}{2}+k_{d1})} =: \Delta Z_\infty. \tag{3.15}$$

Taking the derivative with respect to X_T, one has $\frac{\partial \Delta Z_\infty}{\partial X_T} = \frac{V_z}{\delta^2 k_{d1}}\frac{X_T^2/2+2X_T k_{d1}+k_{d1}^2}{(X_T/2+kd1)^2} > 0$, for all X_T. Therefore, as X_T increases the error ΔZ_∞ increases.

Bound for $\Delta X_I^*(t)$

The activated substrate dynamics X^* evolve in the intermediate timescale. The singular perturbation analysis for the intermediate timescale is performed by setting only $\epsilon_2 = 0$ in (3.7). Let $C = \gamma_c(\hat{X}^*) := \frac{p_T}{k_d}\hat{X}^*$, $C_2 = \gamma_2(\hat{X}^*) := \frac{Y_T}{k_{d2}}\hat{X}^*$, $C_1 = \gamma_1(\hat{Z}, \hat{X}^*) := \frac{\hat{Z}}{\hat{Z}+k_{d1}}(X_T - \hat{X}^* - \gamma_2(\hat{X}^*))$. Variables $\hat{X}^*$ and $\hat{Z}$ denote the dynamics of X and Z in the intermediate timescale. The reduced order dynamics of $\hat{X}^*$ are now obtained by differentiating the slow variable y with respect to time and employing the second equation of (3.7):

$$\frac{dy}{dt} = \frac{d\hat{X}^*}{dt} + \frac{dC_2}{dt} + \frac{dC}{dt},$$

so that

$$\frac{dy}{dt} = \frac{d\hat{X}^*}{dt} + \frac{\partial\gamma_2}{\partial\hat{X}^*}\frac{d\hat{X}^*}{dt} + \frac{\partial\gamma_c}{\partial\hat{X}^*}\frac{d\hat{X}^*}{dt},$$

yielding

$$\frac{d\hat{X}^*}{dt} = \frac{1}{1 + \frac{\partial\gamma_2}{\partial\hat{X}^*} + \frac{\partial\gamma_c}{\partial\hat{X}^*}}(k_1\gamma_1 - k_2\gamma_2)$$

. Further assuming $Z \ll k_{d1}$, and defining $k_1' := k_1/k_{d1}$ and $k_2' := k_2/k_{d2}$, we can write

$$\frac{d\hat{X}^*}{dt} = (1 - R_x)f_x(\hat{X}^*, \hat{Z}), \tag{3.16}$$

where

$$R_x = \frac{p_T/k_d}{p_T/k_d + 1 + Y_T/k_{d2}}, \tag{3.17}$$

$$f_x(\hat{X}^*, \hat{Z}) = \frac{k_1' X_T \hat{Z}\left(1 - \frac{\hat{X}^*}{X_T} - \frac{Y_T}{k_{d2}}\frac{\hat{X}^*}{X_T}\right) - k_2' Y_T \hat{X}^*}{1 + Y_T/k_{d2}}.$$

The reduced order dynamics of $\hat{Z}$ can be obtained by differentiating the slow variable w with respect to time, thus by proof of Case(1) in Lemma 2 of [8], one has that $|\hat{Z}(t, \epsilon_1) - Z(t, \epsilon_1, \epsilon_2)| = O(\epsilon_2/\epsilon_1)$, and $|\hat{X}^*(t, \epsilon_1) - X^*(t, \epsilon_1, \epsilon_2)| = O(\epsilon_2/\epsilon_1)$.

Here, $\hat{X}^*(t, \epsilon_1)$ will be taken as a good approximation of $X^*(t, \epsilon_1, \epsilon_2)$ and we denote

it by $X^*(t)$ with abuse of notation. Also, since $\hat{Z}(t,\epsilon_1)$ and $\tilde{Z}(t)$ are both good approximations of $Z(t,\epsilon_1,\epsilon_2)$, we will use $\tilde{Z}(t)$ in (3.16), given in (3.8), as a good approximation of $\hat{Z}(t)$.

From (3.16), it is notable that the reduced input dynamics have the form of a nominal system with an additive disturbance. The nominal or isolated X^* dynamics are given by setting the retroactivity term $R_x = 0$ ($p_T = 0$) in (3.16) and using (3.10), that is,

$$\frac{dX_I^*}{dt} = f_x(X_I^*, Z_I). \tag{3.18}$$

The dynamics of X_0^* can now be treated as the perturbed version of (3.18) with an input $Z(t) = Z_I(t) + \Delta Z(t)$, where $\Delta Z(t)$ satisfies (3.14):

$$\frac{dX_0^*}{dt} = f_x(X_0^*, Z_I) + h_{\bar{x}}(X_0^*, \Delta Z) \tag{3.19}$$

and $h_{\bar{x}}(X_0^*, \Delta Z)$ is defined as $h_{\bar{x}}(X_0^*, \Delta Z) := \frac{k_1' X_T \Delta Z \left(1 - \frac{X_0^*}{X_T} - \frac{Y_T}{k_{d2}} \frac{X_0^*}{X_T}\right)}{1+Y_T/k_{d2}}$.

Claim 3. Having $\Delta X_{I0}^* := |X_0^*(0) - X_I^*(0)|$, the input error satisfies

$$|\Delta X_I^*(t)| \leq \Delta X_{I0}^* e^{-\lambda_x t} + \frac{C_0^T}{\lambda_x - \lambda_z} e^{-\lambda_z t} + \frac{C_1^T}{\lambda_x - G_z} e^{-G_z t} + \frac{C_2^T}{\lambda_x}, \tag{3.20}$$

where $C_0^T := \left(\frac{k_1' X_T}{1+Y_T/k_{d2}}\right) \Delta Z_0$, $C_1^T := \left(\frac{k_1' X_T}{1+Y_T/k_{d2}}\right) \frac{C_0^z}{\lambda_z - G_z}$, $C_2^T := \left(\frac{k_1' X_T}{1+Y_T/k_{d2}}\right) \frac{C_1^z}{\lambda_z}$, and $\lambda_x := \frac{k_2' Y_T}{1+Y_T/k_{d2}}$.

Proof. Recalling $\Delta Z(t)$ from (3.14), the disturbance $h_{\bar{x}}(X_0^*, \Delta Z)$ satisfies $|h_{\bar{x}}(X_0^*, \Delta Z)| \leq \frac{k_1' X_T}{1+Y_T/k_{d2}} \left(\Delta Z_0 e^{-\lambda_z t} + \frac{C_0^z}{\lambda_z - G_z} e^{-G_z t} + \frac{C_1^z}{\lambda_z}\right)$. The contraction rate of the isolated system (3.18) is found as a positive λ_x such that $m_2\left(\frac{\partial f_x(X_I^*, Z_I)}{\partial X_I^*}\right) \leq -\lambda_x$, for all X_I^*, and Z_I, which results in $\lambda_x = \frac{k_2' Y_T}{1+Y_T/k_{d2}}$. Recalling the constants defined in Claim 3 and using Proposition 1 yields (3.20). □

The steady state input error can be found as

$$\lim_{t \to +\infty} |\Delta X_I^*(t)| \leq \frac{C_2^T}{\lambda_x} = \frac{\Delta Z_\infty}{\rho k_2'/k_1'} =: \Delta X_{I\infty}^*, \tag{3.21}$$

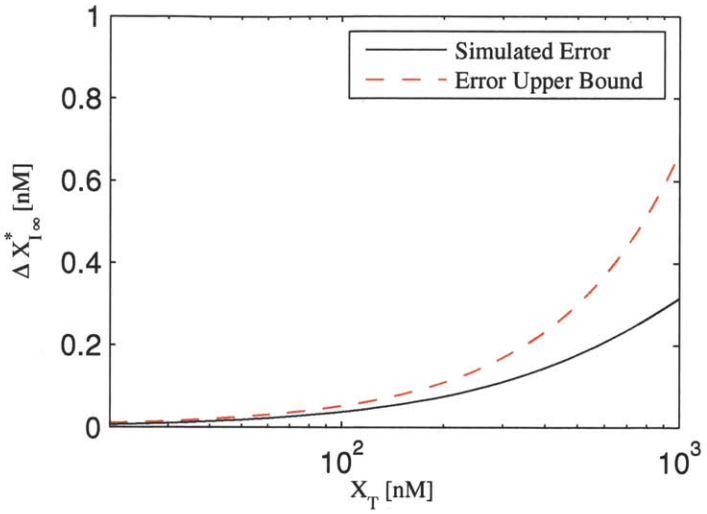

Figure 3-3: Insulation device input error upper bound. Simulated input error from model (3.18) - (3.19) and estimated error upper bound from (3.21). We can see that as the total substrate concentration X_T is increased, the input error increases. This is consistent with the notion of the insulator device creating a retroactivity effect to the input of the upstream module. This error is then propagated to the output protein of the insulator.

which increases as X_T increases. This behavior is captured by Figure 3-3, where the steady state error is also shown as obtained from simulation with a periodic input $k(t)$. One can also see that it lies below the calculated upper bound (3.15) for all values of X_T.

3.3.2 Output error

The dynamics of X^*, subject to both retroactivity effects r and s, will be compared to the dynamics of X_0^* which are only subject to the retroactivity effect r in order to obtain the output error ΔX_0^*. The dynamics of X^* are given by

$$\frac{dX^*}{dt} = f_x(X^*, Z) + h_x(X^*, Z), \tag{3.22}$$

where the expression $h_x(X^*, Z)$ has been defined as

$$h_x(X^*, Z) := -R_x f_x(X^*, Z). \tag{3.23}$$

Equation (3.22) will be treated as the perturbed version of the $X_0^*(t)$ dynamics given in (3.19). In order to apply the robustness result given in Lemma 1 to find a bound on ΔX_0^*, we first need a bound on the perturbation $h_x(X^*, Z)$.

Claim 4. The disturbance $h_x(X^*, Z)$ satisfies

$$|h_x(X^*, Z)| \leq C_0^x e^{-G_x t} + C_1^x, \tag{3.24}$$

where $C_0^x := \left\{ \frac{\frac{p_T}{k_d}\left[k_1' W_x (1+\frac{Y_T}{k_{d2}}) + k_2' Y_T\right]}{\frac{p_T}{k_d}(1+\frac{Y_T}{k_{d2}})^2 + (1+\frac{Y_T}{k_{d2}})^3} \right\} \gamma_x^0$ and $C_1^x := \left\{ \frac{\frac{p_T}{k_d}\left[k_1' W_x (1+\frac{Y_T}{k_{d2}}) + k_2' Y_T\right]}{\frac{p_T}{k_d}(1+\frac{Y_T}{k_{d2}})^2 + (1+\frac{Y_T}{k_{d2}})^3} \right\} \frac{V_x}{G_x K_x \rho}$, defining $\gamma_x^0 := |X(0) - \gamma_x(Z(0))|$, $W_x := \gamma_z(\bar{k}) + \gamma_z^0 + \frac{V_z}{G_z \delta}$, $G_x := \frac{k_2' Y_T}{1 + Y_T/k_{d2} + p_T/k_d}$, $K_x := \frac{k_2'/k_{d2}}{k_1/k_{d1}}$, and $V_x := \delta |Z(0) - \gamma_z(k(0))| + \frac{V_z}{G_z}$.

Proof. See Appendix A-3. □

Claim 5. Having λ_x as the contraction rate of (3.18) and $X_0 := |X^*(0) - X_0^*(0)|$, $|\Delta X_0^*(t)|$ satisfies

$$|\Delta X_0^*(t)| \leq X_0 e^{-\lambda_x t} + \frac{C_0^x}{\lambda_x - G_x} e^{-G_x t} + \frac{C_1^x}{\lambda_x}. \tag{3.25}$$

Proof. Recalling λ_x from Claim 3, one can apply Proposition 1 to get (3.25). □

Assuming $Z(0) = \gamma_z(k(0))$, after a transient the output error is bounded by $\lim_{t\to+\infty} |\Delta X^*(t)| \leq \frac{C_1^x}{\lambda_x} := \Delta X_{0\infty}^*$, where

$$\Delta X_{0\infty}^* = m_x \left[\frac{(k_{d1}\rho + Y_T)^2 2k_1 V_z (k_{d1}\rho)^2}{(2k_{d1}\rho + Y_T)^2} + \frac{\delta^2 k_{d1}\rho[k_2 k_{d1} Y_T + \gamma_z k_1 (k_{d2} + Y_T)]}{Y_T^2 (k_{d2} + Y_T)(2k_{d1}\rho + Y_T)} \right], \tag{3.26}$$

$$m_x = \frac{2k_{d2}^2 p_T V_z}{\delta^3 k_2^2 k_d k_{d1}^2 K_x \rho^2}.$$

Differentiating with respect to Y_T, one has

$$\frac{\partial \Delta X_{0\infty}^*}{\partial Y_T} = -m_x \left[\frac{(k_{d1} + Y_T)\left[8k_1 k_{d1}\rho V_z (k_{d1}\rho + Y_T)^2\right]}{Y_T^3 (2k_{d1}\rho + Y_T)^3} + \frac{\delta^2 \gamma_z k_1 (4k_{d1}^2\rho^2 + 3k_{d1}\rho Y_T + Y_T^2)}{Y_T^3 (2k_{d1}\rho + Y_T)^2} \right.$$
$$\left. + \frac{\delta^2 k_2 k_{d1}[Y_T^2 3k_{d1}\rho + Y_T^3 + 2k_{d1}^2\rho^2(k_{d2} + 2Y_T)]}{Y_T^2 (k_{d2} + Y_T^2)(2k_{d1}\rho + Y_T)^2} \right],$$

making $\frac{\partial \Delta X_{0\infty}^*}{\partial X_T} = \rho \frac{\partial \Delta X_{0\infty}^*}{\partial Y_T} < 0$. Thus, the error decreases as X_T is increased. Figure 3-4 captures this behavior. As it is expected, the calculated upper bound lies above the system error simulation for all values of X_T. Furthermore, without downstream clients ($p_T = 0$), $\Delta X_{0\infty}^* = 0$ since the error only accounts for the retroactivity to the output. In (3.26), since $Y_T = X_T\rho$, $\Delta X_{0\infty}^*$ converges to a value different from zero as $X_T \to \infty$. This is due to the presence of the phosphatase term Y_T/k_{d2} in the R_x expression, which accounts for the phosphatase also placing a load on the output protein X^*. This is different from [3], where the phosphatase term was not accounted for in the retroactivity expression.

3.3.3 Total output error

The total output error can be upper bounded using the triangle inequality $|\Delta X_{TOT}(t)| \leq |\Delta X_0^*(t)| + |\Delta X_I^*(t)|$. Assuming the initial conditions are the same for connected and isolated systems, and having $A(X_T) = \max\left\{\frac{C_0^x}{\lambda_x - G_x}, \frac{C_0^T}{\lambda_x - \lambda_z}, \frac{C_1^T}{\lambda_x - G_z}\right\}$, $\lambda(X_T) = \min\{ G_x, \lambda_z, G_z\}$, and $B(X_T) = \Delta X_{I\infty}^* + \Delta X_{0\infty}^*$, the total error takes the form $|\Delta X_{TOT}^*| \leq A(X_T)e^{-\lambda(X_T)t} +$

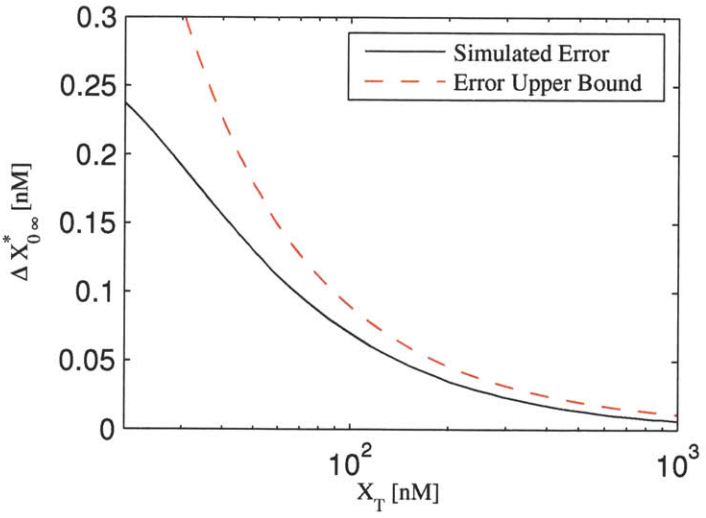

Figure 3-4: Insulation device output error upper bound. Simulated output error from model (3.19) -(3.22), and estimated error upper bound from (3.26). We can see that as the total substrate concentration X_T is increased proportionally to the total phosphatase concentration Y_T, the output error decreases. This is consistent with the notion of retroactivity attenuation through high gain feedback as described in previous works. Thus, high substrate and phosphatase concentration allow for attenuation of retroactivity to the output.

$B(X_T)$. Evaluating the limit at infinite time we have,

$$\lim_{t\to+\infty} |\Delta X^*_{TOT}(t)| \leq \Delta X^*_{I\infty} + \Delta X^*_{0\infty}. \tag{3.27}$$

The optimal selection of X_T, which minimizes both the effects of r and s on signal $X^*(t)$, is given by the minimum of the above expression, which is shown in Figure 3-5. The first term $\Delta X^*_{I\infty}$, defined in (3.21), increases with X_T since it comes from the input error, while the second term, defined in (3.26), decrease as X_T increases since it comes from the output error. This illustrates a tradeoff between the input and output errors. This expression also predicts no error for constant inputs, meaning $V_z = 0$, making retroactivity for the presented model a purely dynamical effect. A final remark on Figure 3-5 is that the bound is tight about the minimum.

Note that if the calculated bounds $\Delta X^*_{I\infty}$ and $\Delta X^*_{0\infty}$ fall in the order of ϵ_2/ϵ_1, then the approximation error due to singular perturbation is not negligible anymore and should be accounted for in the calculations of the error bounds.

3.4 Discussion

This work presents the application of tools from nonlinear systems analysis such as contraction theory and singular perturbation to analyze the tradeoff between input and output retroactivity of a phosphorylation-based insulation device. The analysis shows that while increasing the substrate concentration of the phosphorylation cycle reduces the effect of retroactivity to the output, the cycle becomes a load itself to the upstream system. The error produced by the retroactivity to the input is then propagated to the output, attenuating the output signal. Thus, an optimal substrate concentration was found to be the minimum of a sum of the input and output errors. The results from this work can be used to estimate the minimum upper bound on the error given by the insulation device.

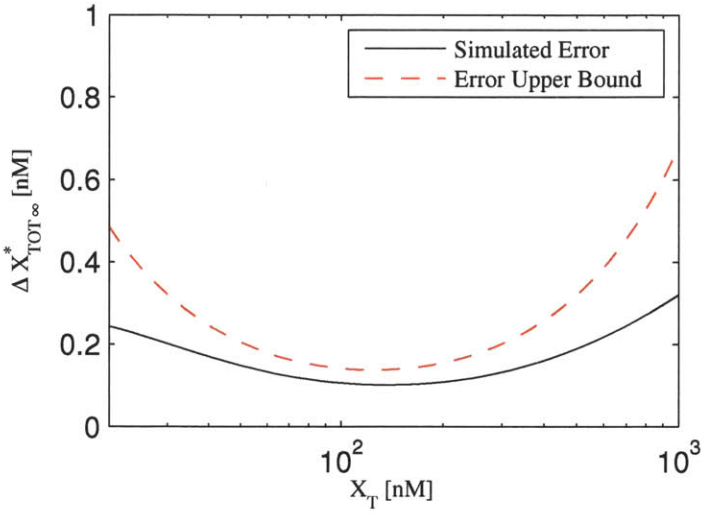

Figure 3-5: Insulation device total error upper bound. Simulated input error from model (3.22) and (3.19) , with no retroactivity to the input, and estimated error upper bound from (3.27). From this plot we can see the tradeoff between attenuation of retroactivity to the input and attenuation of retroactivity to the output. For low substrate concentrations the output error is high due to poor retroactivity to the output attenuation. As the substrate concentration is increased it reaches a minimum value, then for high substrate concentrations the retroactivity to the input has detrimental effects on the insulator output since it creates an error that propagates through the insulator dynamics. Thus, the optimal substrate concentration is given by the minimum of this plot since it minimizes both retroactivity effects.

Chapter 4

Conclusions

This thesis presented the analysis on the successful construction of a phosphorylation based insulation device in *Saccharomyces cerevisae* as well as the relationship of its key constituents, the substrate and phosphatase concentration, with the device output error. The novelty of the device implementation relies on the mixing of slow and fast biochemical networks to achieve the retroactivity attenuation property. This is against the usual notion in systems biology and synthetic biology of analyzing and designing systems in the context of either fast network processes, such as signal transduction, or slow network processes, as in transcriptional regulation. Current experimental studies demonstrated how a transcriptionally activated circuit driving a phosphorylation cascade was able to attenuate retroactivity effects by downstream clients on the device output protein. In the analysis of this experimental system, it was shown through the context of singular perturbation that the quasi-steady state dynamics of the phosphorylation cascade were independent from the load if the constituent reactions are fast enough. Through a flux balance analysis on the quasi-steady state approximation, it was demonstrated that the key parameters in the system where the phosphotransfer rates involving the activation and deactivation of the output protein as well as the total concentrations of substrate and phosphatase. High phosphotransfer and substrate/phosphatase concentration leads to greater attenuation of the retroactivity flux on the overall insulation device dynamics. Thus, the inclusion of an insulation device in a synthetic circuit design allows for the modular composition of systems. This modularity due to the retroactivity attenuation property allows this work to contribute to the bottom up approach in synthetic circuit design.

Furthermore, while increased substrate and phosphatase concentration allow for the elimination of dynamic and steady state dependencies of the device output on the load, it also increases the retroactivity to the input, which might be disruptive to the input device. Using contraction theory, an expression for the upper bound on the output error was provided for an insulation device based on a single phosphorylation cycle. Still, the single cycle model captures the key features from the complex system in the experimental study, including the need for a slow frequency input and the high substrate and phosphatase concentration to increase the output attenuation property. These provide insight into the fundamental limitation that the insulation device has in minimizing both retroactivity effects since, in applications where the input device is highly sensitive to load, the information that wants to be transmitted from the input device to the downstream module might be lost.

The analysis of the experimental results and the theoretical insight on the tradeoff between input and output retroactivity due to substrate and phosphatase concentrations promotes the further development of this research project. The construction of a device where both substrate and phosphatase concentrations are tunable parameters will allow the full characterization of insulation devices based on phosphorylation. It has the potential of illustrating experimentally the tradeoff between input and output retroactivity attenuation providing further guidelines into the optimal implementation of insulation devices in a more general context. Further theoretical work involves the inclusion of the steady state effect due to load in the estimation of the optimal substrate and phosphatase concentration calculation since the current formula allows for optimal prediction due only to dynamic inputs. Also, exploring the effects that high substrate and phosphatase concentration might pose on the cellular metabolism since high phosphorylation activity might lead to high sequestration of the finite available cellular resources.

Appendix A

Proofs

A-1 Consider the system

$$\frac{dZ}{dt} = (1 - R_z(Z))f_z(Z, k(t)) =: g_z(Z, k(t)). \tag{A.1}$$

The upper bound on $h_z(Z, k(t))$ from (3.12) is determined by bounding Z using Lemma 2, then using Lipschitz continuity. Let Z_s be the solution of $g_z(Z_s, k(t)) = 0$, which is given by $Z_s = \gamma_z(k(t)) = k(t)/\delta$. To apply Lemma 2 we need: the bound $\bar{d}$ in (3.3) such that $\left|\frac{\partial \gamma_z(k)}{\partial k}\dot{k}(t)\right| < \bar{d}$, and the contraction rate of (A.1). The bound can be given by

$$\left|\frac{\partial \gamma_z(k)}{\partial k}\dot{k}(t)\right| \leq V_z/\delta. \tag{A.2}$$

The contraction rate G_z of (A.1) is a positive number such that $m_2\left(\frac{\partial g_z(Z,k(t))}{\partial Z}\right) \leq -G_z$, for all Z, and for all $k(t)$. We have shown in Apendix A-2 that $m_2\left(\frac{\partial g_z(Z,k(t))}{\partial Z}\right) \leq m_2\left(\frac{\partial g_z(Z,k(t))}{\partial Z}\right)\Big|_{Z=0}$, making $m_2\left(\frac{\partial g_z(Z,k(t))}{\partial Z}\right) \leq \frac{X_T\left\{2\bar{k}\left[\frac{k_{d2}+Y_T(k_x+1)}{Y_T k_x}\right]-\delta k_{d1}\right\}-\delta k_{d1}^2}{(k_{d1}+X_T)^2}$.

Selecting a Y_T as in the assumption of Claim 1, the X_T factor is smaller than $-\delta k_{d1} X_T/2$, so the contraction rate can be set to

$$G_z := \frac{\delta k_{d1} X_T/2 + \delta k_{d1}^2}{(k_{d1} + X_T)^2}. \tag{A.3}$$

Now Lemma 2 can be applied directly using (A.2) and (A.3). Letting $\epsilon_z(t) := Z(t) - \gamma_z(k(t))$, it follows from Lemma 2 that $|\epsilon_z(t)| \leq e^{-G_z t}|Z(0) - \gamma_z(k(0))| + \frac{V_z}{G_z \delta}$. Finally,

recalling (3.12), one has $|h_z(Z,k(t))| \leq |R_z(Z)||f_z(Z,k(t))|$. From (3.9), since $\frac{\partial R_z}{dZ} < 0$, it follows that

$$|R_z(Z)| \leq \frac{X_T}{X_T + k_{d1}}. \tag{A.4}$$

One has that $|f_z(Z,k(t))| = |f_z(\gamma_z(k(t)) + \epsilon_z(t), k(t))| \leq |f_z(\gamma_z(k(t)),k(t))| + |\Delta_z(t)|$, in which $\Delta_z(t) := f_z(\gamma_z(t) + \epsilon_z(t), k(t)) - f_z(\gamma_z(k(t)),k(t))$. Since $f_z(Z,k(t))$ is Lipschitz continuous in Z with constant $\alpha_z = \delta$, it follows that $|\Delta_z(t)| \leq \alpha_z \epsilon_z(t)$. Also $f_z(\gamma_z(k(t)),k(t)) = 0$, so that

$$|f_z(Z,k(t))| \leq \alpha_z \epsilon_z(t). \tag{A.5}$$

From (A.4) and (A.5) we have $|h_z(Z,k(t))| \leq \frac{X_T\left(\delta|Z(0)-\gamma_z(k(0))|e^{-G_z t} + \frac{V_z}{G_z}\right)}{X_T + k_{d1}}$. Recalling constants C_0^z and C_1^z in Claim 1, we have $|h_z(Z,k(t))| \leq C_0^z e^{-G_z t} + C_1^z$.

A-2 Claim: From system (A.1), $m_2\left(\frac{\partial g_z(Z,k(t))}{\partial Z}\right) \leq m_2\left(\frac{\partial g_z(Z,k(t))}{\partial Z}\right)|_{Z=0}$.

Proof. From (3.9) we see that $(1-R_z)\frac{\partial f_z}{\partial Z} \leq (1-R_z)\frac{\partial f_z}{\partial Z}|_{Z=0} \leq 0$, since $\frac{\partial(1-R_z)}{\partial Z} \geq 0$ and $\frac{\partial f_z}{\partial Z} < 0$.

Thus it suffices to prove that $\frac{\partial}{\partial Z}[f_z \frac{\partial(1-R_z)}{\partial Z}] < 0$. Defining $a := k_{d1} X_T (Y_T k_x / k_{d2})^2$, $b := [1 + Y_T(k_x+1)/k_{d2}]$, and $c := Y_T k_x k_{d1}/k_{d2}$ we have that

$$\frac{\partial}{\partial Z}\left[f_z \frac{\partial(1-R_z)}{\partial Z}\right] = -\frac{2ab(c+bZ)^2(c\delta + 3b\bar{k} - 2b\delta Z)}{[a+(c+bZ)^2]^3} - \frac{a(c\delta - b\bar{k} + 2b\delta Z)}{[a+(c+bZ)^2]^3}$$

which is always negative if $c > b\bar{k}/\delta$ as in the assumptions of Claim 1 and noting that $c^2 < a$. □

A-3 Consider the system

$$\frac{dX^*}{dt} = (1-R_x)\, f_x(X^*, Z) =: g_x(X^*, Z), \tag{A.6}$$

The upper bound on $h_x(X^*, Z)$ from (3.23) can be obtained by bounding X^* using

Lemma 2 and using Lipschitz continuity. and let X_s be the globally unique solution of $g_x(X_s, Z) = 0$ and denote it $X_s = \gamma_x(Z)$. In order to apply Lema 2, we need: the bound $\bar{d}$ in (3.3) given by $\left|\frac{\partial \gamma_x(Z)}{\partial Z}\frac{dZ}{dt}\right| < \bar{d}$ and the contraction rate of (A.6). To obtain bound $\bar{d}$, it was shown in Appendix A-4 that $\left|\frac{\partial \gamma_x(Z)}{\partial Z}\right| \leq \frac{1}{K_x\rho}$, also that the bound on $\left|\frac{dZ}{dt}\right| \leq V_x$ where $V_x := \delta|Z(0) - \gamma_z(k(0))| + \frac{V_z}{G_z}$. Thus $\left|\frac{d\gamma_x(Z)}{dt}\right| \leq \left|\frac{\partial \gamma_x(Z)}{\partial Z}\right| \left|\frac{dZ}{dt}\right| \leq \frac{V_x}{K_x\rho}$. To complete Lemma 2, the contraction rate G_x of (A.6) is determined as a positive number such that $m_2\left(\frac{\partial g_x(X^*,Z)}{\partial X^*}\right) \leq -G_x$, for all X^* and for all Z. One has $m_2\left(\frac{\partial g_x(X^*,Z)}{\partial X^*}\right) \leq -\frac{k_2' Y_T}{1+Y_T/k_{d2}+p_T/k_d}$. Thus, G_x can be defined as $G_x := \frac{k_2' Y_T}{1+Y_T/k_{d2}+p_T/k_d}$. Letting $\epsilon_x(t) := X^*(t) - \gamma_x(Z(t))$ and using Lemma 2, one has

$$|\epsilon_x(t)| \leq e^{-G_x t}|X(0) - \gamma_x(Z(0))| + \frac{V_x}{G_x K_x \rho}. \tag{A.7}$$

Now, recalling (3.23) one has $h_x(X^*, Z) := -R_x f_x(X^*, Z)$, so that $|h_x(X^*, Z)| \leq |R_x||f_x(X^*, Z)|$. Given that $X^* = \gamma_x(Z)+\epsilon_x(t)$, we have that $|f_x(X^*, Z)| = |f_x(\gamma_x(Z)+\epsilon_x(t), Z)| \leq |f_x(\gamma_x(Z), Z)|+|\Delta_x(t)|$, in which $\Delta_x(t) := f_x(\gamma_x(Z)+\epsilon_x(t), Z)-f_x(\gamma_x(Z), Z)$. Recalling W_x from Claim 4, and since $f_x(X^*, Z)$ is Lipschitz continuous with constant $\alpha_x = \frac{k_1' W_x(1+Y_T/k_{d2})+k_2' Y_T}{1+Y_T/k_{d2}}$, one has $|\Delta_x(t)| \leq \alpha_x \epsilon_x(t)$. Also $f_x(\gamma_x(Z), Z) = 0$, so that $|f_x(X^*, Z)| \leq \alpha_x|\epsilon_x(t)|$. It follows that

$$|h_x(X^*, Z)| \leq R_x \alpha_x |\epsilon_x(t)|. \tag{A.8}$$

Recalling variables C_0^x and C_1^x in Claim 4, it follows from (A.7) and (A.8) that $|h_x(X^*, Z)| \leq C_0^x e^{-G_x t} + C_1^x$.

A-4 Claim: From system (A.6), $\left|\frac{d\gamma_x(Z)}{dt}\right| \leq \frac{V_x}{K_x\rho}$.

Proof. Using the Implicit Function Theorem [28], one has $\frac{\partial \gamma_x(Z)}{\partial Z} = -\frac{\partial g_x}{\partial Z}\left(\frac{\partial g_x}{\partial \gamma_x}\right)^{-1}$. It follows that $\frac{\partial \gamma_x(Z)}{\partial Z} = \frac{k_1' X_T\left(1-\frac{\gamma_x}{X_T}-\frac{Y_T}{k_{d2}}\frac{\gamma_x}{X_T}\right)}{k_1' X_T Z\left(\frac{1}{X_T}+\frac{Y_T}{k_{d2}}\frac{1}{X_T}\right)+k_2' Y_T}$, thus $\frac{\partial \gamma_x}{\partial Z} < \frac{\gamma_x}{\partial Z}\big|_{Z=0}$. Recalling K_x in Claim 4 and the definition of ρ, we have that $\frac{\partial \gamma_x}{\partial Z} \leq \frac{1}{K_x\rho}$.

Now, from (3.11), one has $\left|\frac{dZ}{dt}\right| \leq |1 - R_z||f_z|$. Using (3.9), $|1 - R_z| \leq 1$. From (A.5), $|f_z(Z, k(t))| \leq \alpha_z e^{-G_z t}|Z(0) - \gamma_z(k(0))| + \alpha_z \frac{V_z}{G_z \delta}$. Defining $V_x := \delta|Z(0) -$

$\gamma_z(k(0))| + \frac{V_z}{G_z}$, the upper bound on the time derivative of $\gamma_x(Z)$ is given by

$$\left|\frac{d\gamma_x(Z)}{dt}\right| \leq \left|\frac{\partial\gamma_x(Z)}{\partial Z}\right|\left|\frac{dZ}{dt}\right| \leq \frac{V_x}{K_x\rho}.$$

□

Appendix B

Tables

Table B-1: Parameter set shared by insulated and uninsulated systems

	Insulated System		Uninsulated System		
Parameter	Initial Fit	Final Fit	Initial Fit	Final Fit	Unit
δ_X			0.009	0.0065	min^{-1}
k_m	1.0000e-04	1.2000e-4	1.0000e-04	1.2000e-4	μM/min
K_{dox}	3.1030	3.0240	3.1030	3.0240	μM
n_1	1.0	1.0	1.0	1.0	-
k_{on}	5.9999	6.0000	5.9999	6.0000	$[\mu\text{M min}]^{-1}$
k_{off}	0.0187	0.0138	0.0187	0.0138	min^{-1}
k_{sgfp}	0.0012	0.0012	0.0012	0.0012	μM/min
k_g	0.0031	0.0034	0.0031	0.0034	μM/min
K_{gfp}	0.0031	0.0023	0.0031	0.0023	μM
n_2	1.0	1.0	1.0	1.0	-
δ_G	0.0040	0.0040	0.0040	0.0040	min^{-1}
p_T	0.0220		0.0220		μM

Table B-2: Parameter set of the insulated systems

Parameter	Initial Fit	Final Fit	Unit
δ	0.0090	0.0065	min^{-1}
k_p	0.4732	0.9033	$[\mu\text{M min}]^{-1}$
k'_p	0.0040	0.0533	$[\mu\text{M min}]^{-1}$
k_1	3.0000e+03	500.1888	$[\mu\text{M min}]^{-1}$
k_2	500.0000	1.2589e+3	$[\mu\text{M min}]^{-1}$
k_3	65.0760	478.8544	$[\mu\text{M min}]^{-1}$
k_4	212.9052	60.0021	$[\mu\text{M min}]^{-1}$
k_5	0.0040	0.0100	min^{-1}
k_6	0.3264	0.6948	min^{-1}
k_7	0.0040	0.0100	min^{-1}
k_8	0.0040	0.0047	min^{-1}
k_9	0.1000	0.0858	$[\mu\text{M min}]^{-1}$
k_{10}	0.0228	0.7827	$[\mu\text{M min}]^{-1}$
k_{11}	0.0040	0.0073	min^{-1}
k_{12}	19.9998	0.500	$[\mu\text{M min}]^{-1}$
X_T	0.0712		μM
W_T	0.1752		μM

Bibliography

[1] U. Alon, *An introduction to systems biology: design principles of biological circuits.* Chapman & Hall/CRC, 2007.

[2] J. Saez-Rodriguez, S. Gayer, M. Ginkel, and E. D. Gilles, "Automatic decomposition of kinetic models of signaling networks minimizing the retroactivity among modules.," *Bioinformatics (Oxford, England)*, vol. 24, pp. i213–9, Aug. 2008.

[3] D. Del Vecchio, A. J. Ninfa, and E. D. Sontag, "Modular cell biology: retroactivity and insulation.," *Molecular systems biology*, vol. 4, p. 161, Jan. 2008.

[4] S. Jayanthi, K. S. Nilgiriwala, and D. D. Vecchio, "Retroactivity Controls the Temporal Dynamics of Gene Transcription," 2012.

[5] K. H. Kim and H. M. Sauro, "Fan-out in gene regulatory networks.," *Journal of biological engineering*, vol. 4, p. 16, Jan. 2010.

[6] H. M. Sauro and B. Ingalls, "MAPK Cascades as Feedback Amplifiers," pp. 1–21, 2002.

[7] E. Franco, E. Friedrichs, J. Kim, R. Jungmann, R. Murray, E. Winfree, and F. C. Simmel, "Timing molecular motion and production with a synthetic transcriptional clock.," *Proceedings of the National Academy of Sciences of the United States of America*, vol. 108, pp. E784–93, Oct. 2011.

[8] S. Jayanthi, S. Member, and D. D. Vecchio, "Retroactivity Attenuation in Bio-Molecular Systems Based on Timescale Separation," vol. 56, no. 4, pp. 748–761, 2011.

[9] H. K. Khalil, *Nonlinear systems.* Upper Saddle River, NJ: Prentice-Hall, 2002.

[10] A. Belle, A. Tanay, L. Bitincka, R. Shamir, and E. K. O'Shea, "Quantification of protein half-lives in the budding yeast proteome.," *Proceedings of the National Academy of Sciences of the United States of America*, vol. 103, pp. 13004–9, Aug. 2006.

[11] F. Janiak-Spens, P. F. Cook, and A. H. West, "Kinetic analysis of YPD1-dependent phosphotransfer reactions in the yeast osmoregulatory phosphorelay system.," *Biochemistry*, vol. 44, pp. 377–86, Jan. 2005.

[12] P. Jiang, A. C. Ventura, E. D. Sontag, S. D. Merajver, A. J. Ninfa, and D. Del Vecchio, "Load-induced modulation of signal transduction networks.," *Science signaling*, vol. 4, p. ra67, Jan. 2011.

[13] E. Lenssen, N. Azzouz, A. Michel, E. Landrieux, and M. a. Collart, "The Ccr4-not complex regulates Skn7 through Srb10 kinase.," *Eukaryotic cell*, vol. 6, pp. 2251–9, Dec. 2007.

[14] S. Dean, *Achieving specificity in yeast stress responses.* PhD thesis, University of Iowa, 2004.

[15] E. Klipp, B. Nordlander, R. Krüger, P. Gennemark, and S. Hohmann, "Integrative model of the response of yeast to osmotic shock.," *Nature biotechnology*, vol. 23, pp. 975–82, Aug. 2005.

[16] S. a. Chapman and A. R. Asthagiri, "Quantitative effect of scaffold abundance on signal propagation.," *Molecular systems biology*, vol. 5, p. 313, Jan. 2009.

[17] S. Ghaemmaghami, W.-K. Huh, K. Bower, R. W. Howson, A. Belle, N. Dephoure, E. K. O'Shea, and J. S. Weissman, "Global analysis of protein expression in yeast.," *Nature*, vol. 425, pp. 737–41, Oct. 2003.

[18] T. M. Thomson, K. R. Benjamin, A. Bush, T. Love, D. Pincus, O. Resnekov, R. C. Yu, A. Gordon, A. Colman-Lerner, D. Endy, and R. Brent, "Scaffold number in yeast signaling system sets tradeoff between system output and dynamic range.," *Proceedings of the National Academy of Sciences of the United States of America*, vol. 108, pp. 20265–70, Dec. 2011.

[19] M. Carey, C. L. Peterson, and S. T. Smale, *Transcriptional regulation in eukaryotes : concepts, strategies, and techniques.* Cold Spring Harbor, N.Y.: Cold Spring Harbor Laboratory Press, 2009.

[20] M. Schlosshauer and D. Baker, "Realistic protein-protein association rates from a simple diffusional model neglecting long-range interactions, free energy barriers, and landscape ruggedness.," *Protein science : a publication of the Protein Society*, vol. 13, pp. 1660–9, June 2004.

[21] M. Elrod-Erickson, "Binding Studies with Mutants of Zif268. Contribution of individual side chains to binding affinity and specificity in the Zif268 Zinc Finger-DNA complex," *Journal of Biological Chemistry*, vol. 274, pp. 19281–19285, July 1999.

[22] P. Yin, D. Deng, C. Yan, X. Pan, J. J. Xi, N. Yan, and Y. Shi, "Specific DNA-RNA hybrid recognition by TAL effectors.," *Cell reports*, vol. 2, pp. 707–13, Oct. 2012.

[23] R. Phillips, J. Kondev, and J. Theriot, *Physical biology of the cell.* New York: Garland Science, 2009.

[24] W. Lohmiller and J.-J. E. Slotine, "On contraction analysis for non-linear systems," *Automatica*, vol. 34, no. 6, pp. 683–696.

[25] D. Del Vecchio and J.-J. E. Slotine, "A Contraction Theory Approach to Singularly Perturbed Systems," *IEEE Transactions on Automatic Control*, vol. 58, pp. 752–757, Mar. 2013.

[26] E. Klipp, W. Liebermeister, C. Wierling, A. Kowald, H. Lehrach and R. Herwig, *Systems biology.* Wiley VCH, 2009.

[27] W. W. Chen, M. Niepel, and P. K. Sorger, "Classic and contemporary approaches to modeling biochemical reactions.," *Genes & development*, vol. 24, pp. 1861–75, Sept. 2010.

[28] M. J. Marsden, J. E. , Hoffman, *Elementary classical analysis.* W. H Freeman and Company, 1993.